1 **Multiple Determinants and Consequences of Cohesion Fatigue in Mammalian Cells**

2 Hem Sapkota[1,2], Emilia Wasiak[2], John R. Daum[2] and Gary J. Gorbsky[2,3]

1. Department of Cell Biology, University of Oklahoma Health Sciences Center, Oklahoma City, OK 73104, USA

2. Cell Cycle and Cancer Biology Research Program, Oklahoma Medical Research Foundation, Oklahoma City, OK 73104, USA

3 3. Corresponding author

4 **Running Title:** Causes and results of cohesion fatigue

Abstract

Cells delayed in metaphase with intact mitotic spindles undergo cohesion fatigue, where sister chromatids separate asynchronously, while cells remain in mitosis. Cohesion fatigue requires release of sister chromatid cohesion. However, the pathways that breach sister chromatid cohesion during cohesion fatigue remain unknown. Using moderate-salt buffers to remove loosely bound chromatin Cohesin, we show that “cohesive” Cohesin is not released during chromatid separation during cohesion fatigue. Using a regulated protein heterodimerization system to lock different Cohesin ring interfaces at specific times in mitosis, we show that the Wapl-mediated pathway of Cohesin release is not required for cohesion fatigue. By manipulating microtubule stability and Cohesin complex integrity in cell lines with varying sensitivity to cohesion fatigue, we show that rates of cohesion fatigue reflect a dynamic balance between spindle pulling forces and resistance to separation by interchromatid cohesion. Finally, while massive separation of chromatids in cohesion fatigue likely produces inviable cell progeny, we find that short metaphase delays, leading to partial chromatid separation, predispose cells to chromosome missegregation. Thus, complete separation of one or a few chromosomes and/or partial separation of sister chromatids may be an unrecognized but common source of chromosome instability that perpetuates the evolution of malignant cells in cancer.

Introduction

Cells delayed or arrested at metaphase with intact mitotic spindles undergo cohesion fatigue, where sister chromatids separate asynchronously, while the cells remain in M phase (Daum et al., 2011; Stevens et al., 2011). Separated chromatids generated before anaphase likely missegregate or form merotelic attachments that can result in aneuploidy and chromosome breakage. While all cells can undergo cohesion fatigue when arrested at metaphase, the rate of chromatid separation varies significantly within a population of cells and among different cell types, even those closely related. Microtubule pulling forces are essential. Treatment of cells with Nocodazole, a microtubule depolymerizer, completely eliminates cohesion fatigue in mitotic cells arrested by treatment with the proteasome inhibitor, MG132, or by depletion of the SKA3 protein (Daum et al., 2011).

The Cohesin complex normally holds sister chromatids together from DNA replication until anaphase (Michaelis et al., 1997). The major structural elements of the Cohesin ring consists of two Structural Maintenance of Chromosome proteins (SMC3 and SMC1) and cohesin complex component RAD21 that closes the ring. These proteins intersect at three sites, referred to as "gates." Cohesin gates may open during different stages of dynamic Cohesin-chromatin interactions during the cell cycle. For example, Cohesin appears to load onto chromosomes via the opening of the SMC3 and SMC1 hinge interface (Buheitel and Stemmann, 2013) and partially through the SMC3 and RAD21 interface (Murayama and Uhlmann, 2015). To release sister chromatids from each other in mitosis in vertebrates, Cohesin complexes are removed from chromosomes through two mechanisms. In early mitosis until metaphase, the 'prophase pathway' uses Plk1 and Aurora B kinases and the Cohesin removal protein, Wapl, to release a large portion of Cohesin from chromosome arms via opening of SMC3-RAD21 interface of Cohesin. Then at the metaphase-anaphase transition, the protease, Separase, cleaves the RAD21 component of

47 the remaining chromosome-bound Cohesin to induce the final separation of sister chromatids
48 (Waizenegger et al., 2000).

49 In addition to its three core structural ring components, the Cohesin complex contains
50 several regulatory, auxiliary components. One of these has two isoforms called Stromal Antigen
51 1 and 2 (SA1 or SA2) (Solomon et al., 2011; Sumara et al., 2000). Cohesin complexes contain
52 either SA1 or SA2 (Zhang et al., 2008). Cells depleted of either SA1 or SA2 continue to proliferate,
53 but deletion of both is lethal (van der Lelij et al., 2017). Cohesin complexes containing SA1 appear
54 important for arm and telomere cohesion, while Cohesin complexes containing SA2 have more
55 critical roles for centromeric cohesion (Canudas and Smith, 2009). SA2 at centromeres recruits
56 proteins that promote cohesion, including Sororin, Shugoshin (SGO1), and Protein Phosphatase
57 2A (PP2A), that shield centromeric Cohesin from phosphorylation and removal due to the Wapl-
58 mediated prophase pathway (Hauf et al., 2005; McGuinness et al., 2005; Nishiyama et al., 2013).

59 The separation of chromatids in cohesion fatigue requires release of sister chromatid cohesion.
60 However, we do not know if and how the Cohesin complex is breached during cohesion fatigue.
61 Although we and others have shown that depletion of Wapl, a negative regulator of cohesin, prior
62 to mitotic entry, delays cohesion fatigue, it is unclear whether continued Wapl activity is essential
63 for cohesion fatigue after the chromosomes align at the metaphase plate. Previously, we reported
64 that Cohesin protein levels in chromosome fractions remained constant before and after cohesion
65 fatigue (Daum et al., 2011). However, a subsequent study indicated that most, but not all Cohesin
66 in isolated chromosomes was released by a treatment with a moderate concentration of salt
67 (Bermudez et al., 2012). This result suggested that the only the minor, the salt-resistant population
68 comprises the “cohesive” Cohesin that functionally holds sister chromatids together. Currently,
69 we do not comprehensively understand the factors that determine the sensitivity of cells to
70 cohesion fatigue, the mechanism by which cohesion is lost during fatigue, and the consequences
71 of partial and full chromatid separation to downstream chromosome instability.

Results

Cohesin remains bound to chromatids after fatigue.

Current models indicate that Cohesin is released from chromosomes during chromatid separation at anaphase (Supplementary figure 2A and (Kueng et al., 2006; Tomonaga et al., 2000; Uhlmann et al., 2000) Cohesion fatigue also generates separated chromatids. Thus we anticipated that Cohesin should also be released from chromosomes during the process. Nevertheless, in our previous work comparing isolated chromosomes and chromatids prepared from cells before and after fatigue, surprisingly, levels of the core Cohesin subunits associated with chromatin remained unchanged (Daum et al., 2011). However, a potential explanation for this result came from a subsequent study, which revealed that in isolated mitotic chromosomes most Cohesin can be released by treatment with moderate salt (Bermudez et al., 2012). The implication of that work was that only the minor, salt resistant Cohesin was functional in sister chromatid cohesion, and perhaps this small pool was indeed released during fatigue but was too small for detection in our previous study.

We first confirmed that only a fraction of Cohesin remains bound to chromosomes after treatment with moderate salt buffer (Supplementary figure 1B). We then examined whether any changes occurred in the salt-resistant population before and after cohesion fatigue. We treated mitotic cells with MG132 in the absence or presence of Nocodazole for 8 h and then isolated chromosome fractions in moderate salt buffer. As expected, more than 90% of cells treated with MG132 without Nocodazole showed over half of their chromatids separated compared with only 5% of cells treated with MG132 in the presence of Nocodazole. If the salt-resistant Cohesin was released during fatigue, at least a 45% reduction (dotted line figure 1B) in core Cohesin should occur in fatigued samples (MG132 alone) compared to non-fatigued samples (MG132 + Nocodazole). However, immunoblotting for the core Cohesin component, SMC3 revealed no differences Cohesin levels between fatigued and non-fatigued samples (Figures 1A and 1B).

97 Thus, Cohesin release did not occur during cohesion fatigue tracking either the total chromosome-
98 bound population or the salt-resistant population.

99 **Centromeric levels of Shugoshin1 are not critical regulators of sensitivity to cohesion**
100 **fatigue**

101 The Shugoshin1 (SGO1) protein protects centromeric Cohesin from Wapl-mediated
102 release by recruiting protein phosphatase 2A (PP2A) to the centromere region (Gandhi et al.,
103 2006; Liu et al., 2013b; Shintomi and Hirano, 2009; Xu et al., 2009). Changes in SGO1 have been
104 implicated in explaining why different cell lines show differential sensitivity to cohesion fatigue
105 during metaphase arrest (Liu et al., 2013a; Tanno et al., 2015). For our studies, we used two
106 isolates of HeLa cells that exhibit strong differences in the rate of cohesion fatigue
107 (Supplementary figures 4A and 4B). One HeLa cell line, stably expressing histone H2B-GFP,
108 undergoes cohesion fatigue with an average time of approximately 340±127 min at metaphase,
109 while another HeLa cell line, stably expressing histone H2B-mRFP, undergoes cohesion fatigue
110 after an average of 130±55 min. We named these cell lines HeLa-Slow and HeLa-Fast,
111 respectively. We induced metaphase arrest by treating cells with MG132 or with ProTAME, a cell
112 permeant inhibitor of the Anaphase Promoting Complex/Cyclosome (APC/C) (Lara-Gonzalez and
113 Taylor, 2012; Sackton et al., 2014; Zeng et al., 2010).

114 We measured total SGO1 levels in both HeLa-Fast and HeLa-Slow cells and compared
115 SGO1 levels by immunofluorescence in normal prophase, prometaphase or metaphase cells and
116 in cells arrested in metaphase for 6 h (HeLa-Slow) or 3 h (HeLa-Fast). From metaphase-arrested
117 cells, we selected fatigued cells and examined their SGO1 levels. In HeLa-Slow cells, SGO1
118 levels diminished from prometaphase to metaphase, but no further reduction in SGO1 levels
119 occurred with metaphase arrest for 6 h. Cells with separated chromatids showed no reduction in
120 SGO1 levels compared to normal metaphase-arrested cells (Supplementary figure 1D). HeLa-
121 Fast cells showed a similar trend during mitotic progression with SGO1 showing reduced levels

122 at metaphase. In these cells, SGO1 levels were further decreased after 3 h of metaphase delay.
123 However, in cells that underwent cohesion fatigue during the 3 h metaphase delay, SGO1 levels
124 were equal to levels of normal metaphase cells (Supplementary figure 1E). Thus, both cell lines
125 showed a reduction in centromere-associated SGO1 levels as the cells aligned their
126 chromosomes, but SGO1 did not appear to be altered during fatigue. Finally, comparison of total
127 chromosome associated SGO1 levels showed higher levels in HeLa-Fast cells than in HeLa-Slow
128 cells, the opposite that might be expected if SGO1 levels were a major determinant of resistance
129 to cohesion fatigue (Supplementary figure 1C).

130 **Inhibiting Wapl-mediated Cohesin release during early mitosis delays subsequent**
131 **cohesion fatigue.**

132 We and others have previously shown that depletion of Wapl, which mediates Cohesin
133 removal during early mitosis, delays cohesion fatigue (Daum et al., 2011; Stevens et al., 2011).
134 To extend these studies in a system where enhanced Cohesin binding to mitotic chromosomes
135 could be directly monitored, we used Hela cells stably expressing SMC1-GFP (Hou et al., 2007)
136 and examined the effects of Wapl depletion. We depleted Wapl via RNAi, treated the SMC1-GFP
137 cells with ProTAME, and examined cells with clear SMC1-GFP signals on metaphase
138 chromosomes, indicative of those with efficient Wapl depletion (Supplementary figure 2A).
139 Normally, Cohesin released into the cytoplasm by the Wapl-mediated prophase pathway
140 obscures the residual chromosome-bound population, but Wapl depletion results in strong
141 retention of chromosome Cohesin (Gandhi et al., 2006; Haarhuis et al., 2013; Haarhuis et al.,
142 2017; Tedeschi et al., 2013). When Wapl-depleted cells were arrested at metaphase, there was
143 a significant increase in time these cells take to undergo cohesion fatigue (Figure 2A), confirming
144 that Wapl depletion causes increased chromosome association of Cohesin that in turn delayed
145 cohesion fatigue without affecting the total number of cells undergoing fatigue. As another
146 approach we manipulated a competitor of Wapl activity, Sororin, which is normally released from

147 chromatin by mitotic phosphorylation. A Sororin mutant (9A-Sororin) resists mitotic
148 phosphorylation and inhibits Wapl-mediated Cohesin release (Liu et al., 2013b). As expected,
149 cells expressing the 9A mutant form of Sororin showed delayed cohesion fatigue compared to
150 cells expressing wild type Sororin (Figure 2B).

151 **Inhibiting the Wapl pathway or locking cohesin gates after chromosome alignment at**
152 **metaphase does not inhibit cohesion fatigue.**

153 The studies above show that inhibiting the Wapl-mediated Cohesin release during early
154 mitosis slowed cohesion fatigue. Inhibition of Wapl function before mitotic entry increased the
155 levels of salt-resistant Cohesin retained on chromosomes (supplementary figure 2A), and this
156 might fully account for delays in cohesion fatigue. However, it remained possible that Wapl
157 continues to function in opening Cohesin rings during metaphase arrest, contributing to cohesion
158 fatigue after chromosome alignment. We used two distinct approaches to test this possibility. Two
159 mitotic kinases, Plk1 and Aurora B are critical for the function of the Wapl. In our previous work,
160 we showed that chemical inhibition of Plk1 did not block cohesion fatigue, but in that study, the
161 rates of fatigue were not quantified (Daum et al., 2011). Here we used ZM447439, an inhibitor of
162 Aurora B kinase to inhibit Wapl-mediated Cohesin release in HeLa-Slow cells after chromosome
163 alignment at metaphase. Treatment of these cells in early mitosis with 0.5 μM ZM447439 caused
164 significant defects in chromosome alignment, confirming inhibition of Aurora B kinase
165 (Supplementary figure 2B). We added the inhibitor at 2.5 μM, a fivefold higher concentration, one
166 hour after release from Nocodazole to MG132 after most cells had aligned their chromosomes,
167 to avoid disrupting chromosome alignment. Then we tracked cells with tight metaphase plates at
168 the time of ZM447439 addition. The addition of 2.5 μM ZM447439 did not induce loss of
169 chromosome alignment in cells at metaphase, and did not delay cohesion fatigue (Figure 2C).
170 This finding indicated that the continued activity of Aurora B kinase in promoting Wapl activity in
171 metaphase cells does not promote cohesion fatigue in these cells.

172 The Wapl-mediated prophase pathway releases Cohesin by opening the SMC3-RAD21
173 interface or gate. As a stringent test of the role of the Wapl in cohesion fatigue we used three
174 HEK293 cells lines, each expressing a pair of Cohesin ring components tagged with FRB or FKBP
175 proteins that allows locking of SMC3-RAD21 gate, the SMC1-RAD21 gate, and the SMC1-SMC3
176 gate by the addition of Rapamycin (Buheitel and Stemmann, 2013). We depleted endogenous
177 Cohesin proteins and induced expression of the siRNA-resistant fusion proteins. We used
178 chromosome spreads to confirm previously published work that locking the SMC3-RAD21 gate,
179 but not the other gates in early mitosis, inhibited Wapl-mediated release of Cohesin and increased
180 the proportion of chromosomes with unresolved chromosome arms (Supplementary figures 2C
181 and D). We then studied the effect on cohesion fatigue (Figures 2D and E). As expected, when
182 we locked the Cohesin gates by adding rapamycin before cells entered mitosis (Figure 2D top),
183 chromosome spreads showed that cohesion fatigue was inhibited in cells expressing the SMC3-
184 RAD21 pair of Rapamycin-binding proteins, mimicking Wapl inhibition (Figure 2D bottom).
185 Locking the other two gates showed no effect on cohesion fatigue assayed with chromosome
186 spreads. Identical results were found by live cell imaging (Supplementary figure 2E). The results
187 obtained by locking gates before entry into mitosis reveal that gate locking was efficient, that
188 locking the SMC3-RAD21 gate mimicked Wapl depletion in blocking the cohesin removal during
189 prophase and prometaphase, and that Rapamycin-induced dimerization of SMC3-RAD21 in the
190 presence of Wapl was robust and could resist chromatid separation by spindle-pulling forces.

191 Next, we locked the Cohesin gates of Cohesin on chromosomes in metaphase after the
192 normal Wapl-mediated release of unprotected Cohesin during prophase and prometaphase. To
193 accomplish this, we first incubated mitotic cells with nocodazole for 12 h to allow Wapl-mediated
194 cohesin release to be completed (Figure 2E top). We then released cells from nocodazole to
195 MG132 or MG132 plus nocodazole and added Rapamycin to lock each gate. Consistent with our
196 results from Aurora B inhibition, chromosome spreads from cells treated for 6 h with MG132

197 showed that locking any of the Cohesin gates after metaphase alignment did not inhibit cohesion
198 fatigue (Figure 2E bottom). These results indicate that inhibition of the Wapl before/early in mitosis
199 delays cohesion fatigue through an increase in the amount of functional Cohesin retained on
200 chromosomes. However, once cells are at metaphase, after full activity of the Wapl-mediated
201 prophase pathway is complete, inhibition of the Wapl-mediated prophase pathway does not delay
202 fatigue, indicating it is not required for chromatid separation. In addition, locking the other Cohesin
203 gates does not affect fatigue. Thus, transient opening of a single Cohesin gate is unlikely to
204 account for the separation of sister chromatids in cohesion fatigue for cells we have analyzed.

205 **Compromised Cohesin accelerates cohesion fatigue.**

206 Cohesin-chromatin interactions are highly regulated throughout cell cycle (Bermudez et
207 al., 2012; Gandhi et al., 2006; Lara-Gonzalez and Taylor, 2012; Liu et al., 2013a; Whelan et al.,
208 2012; Xu et al., 2014). In early mitosis, Cohesin is removed from chromosome arms by the Wapl-
209 mediated prophase pathway (Gandhi et al., 2006; Kueng et al., 2006; Nishiyama et al., 2010;
210 Nishiyama et al., 2013; Shintomi and Hirano, 2009). In cells arrested in mitosis for long periods,
211 Cohesin removal separates chromosome arms, which generates the classic "X-shape"
212 chromosomes seen in chromosome spreads (Supplementary figure 3A). We previously found that
213 under normal conditions, cohesion fatigue initiates at kinetochores then propagates down the
214 chromosome arms. Thus, Cohesin loss and arm separation should increase cell susceptibility to
215 cohesion fatigue. To test this idea, we used chromosome spreads to compare rates of cohesion
216 fatigue in LLC-PK cells after arresting cells in mitosis for 5 or 11 h with Nocodazole. After
217 Nocodazole arrest, cells were washed then placed in fresh media containing MG132 and then
218 processed for chromosome spreads immediately (0 h), 3 h or 6 h later (Figure 3A left). Cells
219 arrested in Nocodazole for 11 h had significantly increased cohesion fatigue compared to cells
220 arrested for just 5 h (Figure 3A right). In contrast, cells harvested at 0 h, 3 h or 6 h after being
221 maintained in MG132 plus Nocodazole showed very few separated chromatids. We hypothesized

222 that arrest in Nocodazole might decrease the level of salt-resistant Cohesin on chromosomes.
223 Quantification of western blots showed a modest decrease in chromosome-bound Cohesin levels
224 comparing chromosomes from cells arrested for 5 and 11 h (Supplementary figure 3C). These
225 results indicate that longer mitotic arrest, without spindle pulling forces, primes cells to undergo
226 faster cohesion fatigue.

227 These results indicated that the increased time spent in mitosis leads to a higher
228 propensity for cohesion fatigue. As a complimentary method to test this idea, we compared onset
229 of cohesion fatigue in cells that reach full metaphase quickly with those where chromosome
230 alignment is delayed. To increase the proportion of cells with alignment delays, we treated cells
231 with 1.5 uM S-Trityl-L-cysteine (STLC), an inhibitor of mitotic motor kinesin Eg5 (Skoufias et al.,
232 2006). When we measured the time from full metaphase alignment to cohesion fatigue, cells with
233 the slowest alignment, and thus with longer times spent in prometaphase, showed faster cohesion
234 fatigue (Supplementary figure 3B).

235 The Cohesin subunit SA2 is thought to promote cohesion specifically at centromeres
236 (Canudas and Smith, 2009). Unlike Sgo1 depletion where sister chromatids separate without
237 spindle pulling forces, depletion of SA2 caused increased interkinetochore distances only in the
238 presence of intact spindles (Kleyman et al., 2014) suggesting defective cohesion maintenance
239 rather than compromised cohesion establishment. If so, then depletion of SA2 should accelerate
240 cohesion fatigue. We investigated the consequences of SA2 loss using HCT116 cells in which
241 the STAG2 gene, which codes for SA2, had been deleted by homologous recombination
242 (Solomon et al., 2011). Chromosomes from SA2 knockout cells showed reduced amounts of the
243 Cohesin ring components, SMC3 and RAD21, compared to parental HCT116 cells
244 (Supplementary figure 3E). Metaphase arrest for 3 or 6 h caused increased separation of
245 chromatids in chromosome spreads of SA2 knockout cells compared to parental cells (Figure 3B).
246 Inclusion of nocodazole to disrupt spindle microtubules abrogated the differences in chromatid

247 separation in SA2 knockout and parental cells. Thus, loss of the Cohesin regulatory component,
248 SA2, increases the susceptibility of cells to cohesion fatigue in the presence of spindle pulling
249 forces. Because SA2 helps to resist cohesion fatigue, we hypothesized that its release might
250 accompany fatigue. We analyzed chromosome fractions from HeLa cells by western blot before
251 and after fatigue but found no reduction in the amount of chromosome-bound SA2 after chromatid
252 separation (Figure 3C).

253 **Modulating microtubule stability alters rates of cohesion fatigue.**

254 Previously we showed that complete disruption of spindle microtubules blocked cohesion
255 fatigue, which indicated that spindle pulling forces were essential (Daum et al, 2011). However, it
256 was unclear the degree to which the rate of cohesion fatigue might be sensitive to microtubule
257 dynamic turnover. To alter microtubule dynamics while maintaining intact spindles, we used 5 nM
258 Nocodazole and 1.5 nM Taxol, concentrations that slow but do not block progression of control
259 cells through mitosis (Supplementary figure 4C). We measured the elapsed time from metaphase
260 to chromosome scattering (fatigue) in cells arrested at metaphase. Treatment with 5 nM
261 Nocodazole marginally delayed chromosome alignment, but significantly slowed cohesion fatigue
262 in both HeLa-Slow and HeLa-Fast cells (Figure 4A). Correspondingly, partial stabilization of
263 spindle microtubules with 1.5 nM Taxol led to faster cohesion fatigue in both cell types (Figure
264 4B). When viewed as percentages, HeLa-Slow and HeLa-Fast cells showed comparable delay in
265 cohesion fatigue when treated with Nocodazole and comparable acceleration when treated with
266 Taxol.

267 To reduce spindle tension we treated cells with low concentrations of the Eg5 inhibitor
268 STLC (Skoufias et al., 2006). At high concentrations, STLC induces collapse of spindle poles.
269 But, at reduced concentrations, spindles can be maintained with decreased interpolar distance
270 and diminished spindle tension (Vallot et al., 2017). The decrease in spindle tension should
271 reduce the outward force on kinetochores. In control cells, 1.5 uM STLC caused only a slight

272 delay in normal mitotic progression (Supplementary figure 4D). In cells arrested at metaphase,
273 STLC treatment led to significantly slower cohesion fatigue in both HeLa-Slow and HeLa-Fast
274 cells (Figure C).

275 **Fatigued chromatids can congress to the metaphase plate.**

276 Normally metaphase in mitosis requires approximately 10 to 30 min before synchronous
277 separation of sister chromatids in anaphase occurs, followed by mitotic exit. In contrast, when
278 cells are experimentally delayed at metaphase, chromatids pull apart slowly and asynchronously
279 while cells remain in mitosis (Figure 5A). The rate of chromatid separation varies widely among
280 different cell lines. Chromosome spreads of cells arrested for a few to several hours (depending
281 on the cell line) show complete separation of most chromosomes (Figure 1B). Typically, in cells
282 that have undergone cohesion fatigue, some chromatids are oriented near the poles but many
283 appear clustered near the metaphase plate (Figure 5A, last panel). To understand the behavior
284 of chromatids during cohesion fatigue we used high resolution lattice light sheet microscopy to
285 track chromatid movement after cohesion fatigue. Live imaging of LLC-Pk cells stably expressing
286 GFP-Topoisomerase IIα, which marks both kinetochores and chromosome arms, revealed that
287 partially and completely separated chromatids oscillate toward and away from the spindle
288 midplane (Compare normal mitosis in Supplemental Video 1 and cohesion fatigue in
289 Supplemental Video 2). Thus, unpaired kinetochores on chromatids separated by cohesion
290 fatigue can subsequently align near the metaphase plate. This is likely due to formation of
291 merotelic attachments of single kinetochores to microtubules from both poles and to microtubule-
292 based ejection forces from the poles impacting chromatid arms.

293 **Short delays at metaphase induce partial separation of chromatids at their kinetochores.**

294 Chromatid separation in cohesion fatigue is progressive, initiating at the kinetochores then
295 advancing distally along the chromosome arms (Daum et al., 2011). To evaluate the time-course

296 of chromatid separation after short delays, we tracked the interkinetochore distance between
297 sister chromatids in LLC-PK cells. We detected significant separation of kinetochores in cells
298 treated with MG132 for 3 h (Figure 6A) In most cells arrested for 3 h, sister chromatid arms
299 remained attached, but kinetochores were significantly separated with many showing separations
300 of more than 3 μm versus 1.75 μm in control metaphase cells and 0.7 μm in cells treated with 330
301 nM nocodazole (Figure 6A, 6B and Supplementary figure 5A). Like LLC-PK cells, HeLa-Slow cells
302 also showed increased interkinetochore distances when delayed at metaphase for 3 h
303 (Supplementary figure 5B). To examine the dynamics of chromatid separation in detail, we used
304 live cell imaging to monitor metaphase-arrested LLC-PK cells expressing GFP-Topoisomerase
305 IIα. As anticipated from the analysis of fixed cells, live cell tracking showed wider average
306 distances between sister kinetochores in cells arrested at metaphase with MG132 for 3 hours
307 compared to untreated control cells or cells treated for only 1 hour (Supplementary figure 5C).
308 Moreover, cells treated with MG132 for 3 h showed a significantly larger range of stretching
309 between sister kinetochores compared to cells treated for only 1 h. In metaphase of untreated
310 cells or cells treated with MG132 for 1 h, the average distance between sister kinetochores varied
311 over an average range of about 0.4 μm as sister kinetochores oscillated together and apart. In
312 contrast, cells arrested at metaphase for 3 h showed a range of stretching between sister
313 kinetochores of 1 μm or more (Figure 6C). Overall, moderate delays at metaphase cause
314 abnormal separation of kinetochores.

315 **Partial separation of chromatids induces chromosome segregation defects.**

316 Transient delays in anaphase onset after most chromosomes have aligned at the
317 metaphase plate often occur because one or more chromosomes lag in congression, even in an
318 unperturbed, normal mitosis. To examine the immediate impact of partial chromatid separation
319 that may occur during a transient delay, we arrested cells at metaphase, then released them into
320 anaphase. We arrested LLC-PK cells with 5 μM MG132 for 3 h. Cells were washed into fresh

321 medium without drug and then fixed 3.5 h later when most had entered anaphase. We examined
322 every cell that entered anaphase for lagging chromosomes, anaphase bridges or micronuclei
323 (Figure 7A left). Cells arrested at metaphase for 3 h with MG132 treatment exited mitosis with an
324 error rate of ~44%. Cells treated and released after a treatment with both MG132 and Nocodazole
325 showed segregation errors in 18% of anaphases, significantly lower than MG132 treatment alone
326 (Figure 7A right). Cells treated and released from a 3 h Nocodazole arrest exhibited a slightly
327 elevated error rate of 7%. Untreated control cells exited mitosis with a missegregation rate of
328 ~4%. Because mitotic exit after release from MG132 requires approximately 3.5 h while recovery
329 from Nocodazole takes only 30-60 min, cells released from the combination of MG132 and
330 Nocodazole arrest at metaphase with an intact spindle for approximately 3 h. This finding is
331 consistent with the higher rate of anaphase defects in these cells compared with controls. We
332 also compared the accumulation of segregation defects in cells arrested at metaphase for
333 different durations. We treated LLC-PK cells with MG132 for 1 or 4 h, released them in fresh
334 medium and then evaluated the anaphases. In cells arrested for 1 h, 13% of the anaphases
335 showed segregation errors, while in cells arrested for 4 h, 55% of revealed errors (Supplementary
336 figure 6A).

337 Not all anaphase chromosome segregation errors cause aneuploidy, as some lagging
338 chromosomes are properly incorporated into daughter nuclei. However, missegregated
339 chromosomes often decondense separately to form micronuclei that persist for long periods in
340 daughter cells and can induce catastrophic DNA damage (Crasta et al., 2012; Hatch et al., 2013;
341 Thompson and Compton, 2011; Zhang et al., 2015). We tested whether short metaphase delays
342 increase the incidence of micronuclei. We quantified the number of micronuclei in LLC-PK cell
343 cultures 24 h after transient arrests with MG132 or Nocodazole for 1 h and 3 h. Cells delayed at
344 metaphase with MG132 treatment for 3 h exhibited significantly higher numbers of micronuclei
345 compared to cells arrested for 1 h or cells treated with nocodazole for 3 h (Figures 7B and C).

346 To map the effects of short metaphase delays in greater detail, we used video microscopy.
347 To achieve metaphase delays of varying lengths, we treated cells with 10, 20 or 30 μM ProTAME.
348 ProTAME is a cell permeable inhibitor of the APC/C (Zeng et al., 2010). ProTAME delayed cells
349 at metaphase in a dose-dependent manner for varying durations (Supplementary figure 6B).
350 These ProTAME-induced metaphase delays were followed by three outcomes: 1) normal
351 anaphase and mitotic exit, 2) defective anaphase involving lagging chromosomes, anaphase
352 bridges, or micronuclei or 3) cohesion fatigue (Figure 8A). Cells delayed at metaphase for less
353 than 2 h had a low incidence (14%) of anaphase defects. The number of cells showing defective
354 anaphase increased to 37% in cells delayed for 3 h and to approximately 58% in cells delayed for
355 4 h. With longer arrest durations, the number of cells exhibiting defective anaphase declined,
356 while the number of cells that underwent cohesion fatigue increased (Figures 8B and 8C). Cells
357 exhibiting normal anaphase were delayed at metaphase an average of 134 ±111 min, while cells
358 showing at least one kind of chromosome segregation defect were delayed for 199 ±106 min.
359 Cohesion fatigue occurred in cells arrested at metaphase for 370 ±105 min (Supplementary figure
360 6C). Thus, cells showed an increased frequency of segregation errors that correlated with the
361 duration of metaphase arrest but then exhibited cohesion fatigue after extended times at
362 metaphase. Cells with massive chromatid separation did not generally enter anaphase, likely due
363 to reactivation of the spindle checkpoint. Overall, limited separation of chromatids caused by
364 transient metaphase delay produces chromosome segregation defects in anaphase and often
365 generates micronuclei.

366

367 **Discussion:**

368 Our data reveal that breaching of sister chromatid cohesion that accompanies cohesion
369 fatigue does not require release of core Cohesin ring components from chromatids. It also does
370 not appear to exploit a specific protein-protein interface in the Cohesin ring. More specifically, the
371 Wapl-mediated opening of cohesin rings is not required after metaphase arrest to separate sister
372 chromatids in cohesion fatigue. In contrast, loss of Wapl activity in early mitosis leads to increased
373 retention of Cohesin on metaphase chromosomes, which does inhibit subsequent cohesion
374 fatigue. Experimental manipulations that compromise Cohesin integrity in mitotic chromosomes
375 accelerate cohesion fatigue. Our studies demonstrate the dynamic tension of the mitotic spindle,
376 specifically the pulling forces acting on kinetochores is countered by the resistance of Cohesin
377 that holds chromatids together. The rate of chromatid separation in cells delayed at metaphase
378 yields a quantitative measure of these two antagonistic components. Our studies also reveal that
379 partially or fully separated chromatids can travel to the spindle equator. This competence for the
380 kinetochores of unpaired chromatids to congress to the metaphase plate was first described by
381 (Brinkley et al., 1988). Finally, we show that in contrast to complete chromatid separation that
382 accompanies cohesion fatigue, even relatively short metaphase delays can result in partial
383 chromatid separation that lead to defects in chromosome segregation during the subsequent
384 anaphase.

385 In mitosis in vertebrate cells, most Cohesin is released from chromosomes through the
386 activities of mitotic kinases and the Wapl protein which act during early mitosis. Of the remaining
387 Cohesin that remains bound to isolated mitotic chromosomes, most can be released by treatment
388 with moderate levels of salt (Bermudez et al., 2012). Although not proven, we speculate that the
389 functional or “cohesive” Cohesin that holds sister chromatids together reflects the minor, salt-
390 resistant population. The precise molecular nature of Cohesin interactions with chromatin remains
391 a topic of research and debate. For sister chromatid cohesion, most models are variations on two

392 general modes of Cohesin/chromatin interaction termed “embrace” or “handcuff” models
393 (reviewed in (Skibbens, 2016). Embrace models propose that both sisters are contained within
394 the same Cohesin ring, while handcuff models suggest sister chromatids are enclosed in separate
395 rings that are linked together. Recently a new model of chromatin binding by Cohesin was
396 reported, termed “hold-and-release” (Xu et al., 2018). The hold-and-release model proposes that
397 DNA is sandwiched by arched coiled-coils of SMC components rather than entrapped within a
398 ring. Although sister chromatids undergo separation during cohesion fatigue, we found no change
399 in the amount of salt-stable, core Cohesin components bound to chromosomes before or after
400 chromatid separation (Figure 1). This surprising result suggests that salt-resistant Cohesin is not
401 released from chromatids during their separation. This outcome is most consistent with the
402 handcuff models or the newly suggested hold-and-release model of interchromatid cohesion since
403 these do not necessarily require Cohesin release at chromatid separation. However, there are
404 other potential explanations for our findings. One is that sister chromatid cohesion is mediated
405 only by a minor subfraction of the salt-resistant Cohesin, which is indeed released during cohesion
406 fatigue at levels we cannot detect. Recent work in Drosophila, where total Cohesin levels were
407 genetically regulated, shows that expression of very low levels of Cohesin can maintain normal
408 sister chromatid cohesion at metaphase (Oliviera, personal communication). Another possibility
409 to explain our results is that Cohesin interactions with chromatin are remodeled during fatigue
410 from binding sister chromatids together to binding chromatin segments within a single chromatid.
411 This possibility has been proposed to explain centromere structure in budding yeast (Yeh et al.,
412 2008) and chromatin immunoprecipitation studies in yeast suggest that Cohesin may be able to
413 break and reform chromatid linkages during mitosis (Ocampo-Hafalla et al., 2007). Alternatively,
414 salt-resistant Cohesin might be released during chromatid separation only to rebind onto the
415 separated chromatids later. Finally we cannot exclude the possibility that DNA damage generated
416 during cohesion fatigue could recruit Cohesin during separation (Unal et al., 2004).

417 Another potential explanation for the retention of Cohesin on chromatids during cohesion
418 fatigue is that protein-protein interactions among proteins comprising the Cohesin ring may open
419 transiently. Opposing poleward-directed tension may exploit these transient openings, allowing
420 sister chromatids to slip apart. Separation would initiate at the kinetochores then progress down
421 the length of the chromosome arms, the exact behavior observed in time lapse imaging (Daum et
422 al., 2011). However, in our current study, after allowing the normal activity of the Wapl-mediated
423 Cohesin release in prometaphase, locking of individual gates of Cohesin complexes at metaphase
424 did not inhibit cohesion fatigue (Figure 2E). This evidence suggests that neither the SMC3-
425 RAD21, Wapl gate nor the SMC1-SMC3 and the SMC1-RAD21 gates are individually required
426 for cohesion fatigue. Because we cannot lock multiple gates at the same time, we cannot eliminate
427 the possibility that transient openings of multiple Cohesin gates contributes to cohesion fatigue.
428 In our previous study we showed, by siRNA depletion, that background Separase activity did
429 slightly affect the timing of cohesion fatigue but was not required (Daum et al., 2011). This
430 evidence, along with our current Aurora B inhibition studies (Figure 2C) and gate locking
431 experiments suggest that the mechanism of cohesion fatigue is likely a novel, yet undiscovered
432 pathway of breaching sister chromatid cohesion. Thus, the phenomenon of cohesion fatigue
433 provides an additional tool to study the nature of Cohesin interaction with chromatin.

434 Our studies reveal that the amount of Cohesin retained on chromosomes dictates the rate
435 of cohesion fatigue. While Wapl activity is not required for cohesion fatigue, previous work showed
436 that siRNA-mediated depletion of Wapl decreased the rate and extent of cohesion fatigue (Daum
437 et al., 2011; Stevens et al., 2011). We tested the idea that this was due to increased retention of
438 Cohesin on mitotic chromosomes by using HeLa cells stably expressing SMC1-GFP and showed
439 directly that cohesion fatigue is delayed in cells where mitotic chromosomes show enrichment of
440 Cohesin after Wapl depletion prior to mitotic entry. We also showed that expression of the Wapl
441 antagonist, Sororin, mutated to be resistant to removal by mitotic phosphorylation, also delays

442 cohesion fatigue. These experiments confirm that inhibition of Wapl-mediated prophase pathway
443 before mitotic entry enriches Cohesin on chromosomes and delays cohesion fatigue (Figures 2A
444 and 2B).

445 While our results show that the Wapl-mediated cohesin removal is not essential for
446 cohesion fatigue, it may still influence timing. Complete disruption of spindle microtubules
447 eliminates cohesion fatigue. However, extended arrest in the absence of microtubules renders
448 cells more sensitive to subsequent cohesion fatigue when metaphase spindles are allowed to
449 form (Figure 3A). Over time in cells arrested with depolymerized spindles, chromosome-
450 associated Cohesin may diminish through continued Wapl-mediated Cohesin release and/or
451 background separase activity. In support of this idea, we found diminished Cohesin levels on
452 chromosomes isolated from cells treated with Nocodazole for longer times (Supplementary figure
453 3C).

454 Two previous studies reported that experimentally induced metaphase delays would
455 reduce immediate chromosome segregation errors (Cimini et al., 2003; Ertych et al., 2014).
456 However, our detailed analyses indicated the opposite, that transient metaphase delays increase
457 the incidence of segregation defects during anaphase (Figures 7 and 8). The reason for this
458 discrepancy is not clear, but the previous reports used different cell lines and different
459 experimental conditions. Consistent with the previous studies, we found that very short
460 metaphase delays did not increase the chromosome segregation errors (Supplementary figure
461 6C). Our results point to a critical threshold of metaphase arrest and accompanying kinetochore
462 separation that may be required before the delay becomes detrimental. In our experiments
463 increased kinetochore separation abrogates the normal back-to-back orientation of sister
464 kinetochores allowing greater chances for merotelic attachments of single kinetochores to both
465 spindle poles. Such merotelic kinetochore attachments have been shown to increase the
466 incidence of anaphase defects (Cimini et al., 2003; Salmon et al., 2005; Thompson and Compton,

467 2011). Cohesion fatigue that generates chromatid separation in several chromosomes likely
468 compromises cell viability either through cell cycle arrest mediated by the spindle checkpoint or
469 through catastrophic chromosome missegregation if cells exit mitosis. The more subtle errors that
470 accompany partial chromatid separation for cells with shorter delays at metaphase may produce
471 segregation defects that can propagate in daughter cells.

472 Although certain cells, notably some cancer cell lines, exhibit high degrees of chromosome
473 instability, most dividing cells in culture show low rates of spontaneous segregation errors that
474 can manifest in several ways (Thompson and Compton, 2008). As with the other errors, we
475 observe spontaneous cohesion fatigue in normal control cells at low frequency (data not shown).
476 Cells that undergo substantial cohesion fatigue with many separated chromatids are likely to die,
477 because separated single chromatids elicit spindle checkpoint signaling (Lara-Gonzalez and
478 Taylor, 2012), which promotes continued mitotic arrest and cell death. Even if they survive and
479 divide after delay, the progeny cells would have highly abnormal chromosome content and would
480 likely be inviable. In this study we also focused on less extreme circumstances, where shorter
481 delays at metaphase allowed sister chromatids to partially separate before anaphase onset
482 (Figure 6).

483 Cohesin complexes contain one of two auxiliary “Stromal Antigen” components, SA1 or
484 SA2. In HCT116 and RPE1 cells, depletion of SA2 causes significant increases in lagging
485 chromosomes (Kleyman et al., 2014). Furthermore, in HCT116 cells, knockout of the Stag2 gene,
486 which codes for SA2, does not strongly affect normal mitotic progression but may increase the
487 incidence of aneuploidy (Solomon et al., 2011). We found that HCT116 cells lacking SA2
488 underwent faster cohesion fatigue compared to parental HCT116 cells (Figure 3B). However, it
489 does not appear that release of SA2 accompanies cohesion fatigue in normal cells, since
490 chromatin-associated SA2 does not decrease during metaphase arrest or after chromatid
491 separation (Figure 3C). Inactivating mutations in the Stag2 gene are correlated with aneuploidy

492 in some cancers (Solomon et al., 2011). We propose that an increased propensity for full or partial
493 chromatid separation due to cohesion fatigue may contribute to aneuploidy in cells with mutations
494 in Stag2.

495 Previous studies suggested that cells prone to undergo rapid cohesion fatigue showed
496 altered distribution and reduced levels of the Cohesin protector protein, SGO1 (Tanno et al.,
497 2015). However, both fast and slow fatiguing HeLa cells exhibited no significant reduction in
498 SGO1 protein during cohesion fatigue when compared to metaphase levels (Supplementary
499 figures 1D and 1E). SGO1 levels were higher at metaphase in HeLa-Fast cells compared to HeLa-
500 Slow cells, the opposite one might expect if Sgo1 levels regulated the rate of cohesion fatigue.
501 Taken together, our observations indicate that breaching cohesion during cohesion fatigue may
502 not require canonical Cohesin removal mechanisms, such as the Wapl pathway or the activity of
503 Separase. However, we believe it is highly likely that these mechanisms may influence the
504 sensitivity and rates of cohesion fatigue in different cells and under different conditions.

505 Metaphase is a point of balance between microtubule-dependent pulling forces that
506 separate chromatids versus cohesive forces that hold chromosomes together. We show that
507 mitotic spindle microtubule dynamics affect cohesion fatigue, likely by modulating spindle-pulling
508 forces. Low concentrations of Taxol accelerate fatigue, while low concentrations of Nocodazole
509 slow it. Partial inhibition of Eg5 kinesin with STLC likely compromises overall spindle tension to
510 relax spindle-pulling force and slow cohesion fatigue (Figure 4). These results highlight the roles
511 of robust and dynamic microtubules and sufficient spindle-pulling forces to separate sister
512 chromatids during cohesion fatigue.

513 While normally transient, metaphase can be delayed. Our data suggest that many factors
514 contribute to cell sensitivity to cohesion fatigue including the various canonical Cohesin
515 regulators. However, a complete understanding of the primary molecular mechanisms underlying
516 chromatid separation during cohesion fatigue remains unresolved and may reflect an incomplete

517 understanding of sister chromatid cohesion. Future studies of cohesion fatigue may provide
518 insight into the nature of Cohesin complex-chromatin interactions. While complete chromatid
519 separation of many chromosomes will likely result in cell death or inviable progeny cells, complete
520 separation of one or a few chromosomes and/or partial chromatid separation may be an important
521 source of genomic instability that perpetuates the evolution of malignant cells in cancer.

522 **Material and methods:**

523 **Cell culture and drug treatments:** HeLa, LLC-PK, HCT116 and HEK293 cells were cultured in
524 flasks in DMEM-based media supplemented with 2 mM HEPES, non-essential amino acids
525 (NEAA), sodium-pyruvate, 1X penicillin-streptomycin (P/S, Corning, 30-002-CI) and 10% FBS.
526 Cells were maintained at 37°C in 5% CO_2 in a water-jacketed incubator. Cells were subcultured
527 every other day and were used within 6 months of thawing from liquid nitrogen. Unless otherwise
528 specified, drugs were applied at the following concentrations: Nocodazole: 330 nM, MG132: 25
529 μM, ProTAME: 25 μM, Rapamycin: 100 nM, ZM447439: 2.5 uM. All cell lines were routinely tested
530 for mycoplasma. HeLa cells, LLC-PK cells and HCT116 cells were mycoplasma free. The
531 HEK293 cells were found to be mycoplasma positive. Unfortunately, all the stock cultures, even
532 the earliest isolates at the laboratory of origin were found to be mycoplasma positive. We used
533 several approaches designed to cure the mycoplasma contamination, but these were
534 unsuccessful.

535 **Chromosome/chromatin isolation:** Subconfluent cultures of HeLa cells were treated with
536 Nocodazole for 12 - 16 h, then mitotic cells were collected by shake-off. Cells remaining in the
537 flasks (interphase cells primarily in G2) were collected by trypsinization. Cells were centrifuged in
538 50 ml tubes at 200 Xg for 4 min and re-suspended in warm media at 1X10^6 cells/ml. 4x10^5
539 cells were aliquoted into 1.5 ml micro-centrifuge tubes and centrifuged at 200 Xg for 5 min. The
540 cell pellet was then lysed with cold Extraction Lysis Buffer (ELB) by repeated pipetting. The ELB
541 contained PHEM buffer: 60 mM PIPES, 25 mM HEPES, 10 mM EGTA and 4 mM $MgCl_2$ with 0.1
542 M NaCl, 1% CHAPS, 1mM DTT, and 1:200 protease inhibitor (Sigma, P8340). Lysed cells were
543 incubated for 20 min in ice then centrifuged at 1400 Xg for 10 min. A fraction of soluble
544 supernatant was saved. The pellets were subjected to two more cycles of resuspension in ELB
545 and centrifugation.

546 **Western blot:** Supernatant and chromatin pellets were dissolved in 1X loading buffer (1X LDS
547 sample buffer (Thermofisher, NP007) + 50 mM DTT). Equivalent cell numbers were loaded on 4-
548 12% NuPAGE gels, electrophoresed at 50 V for 7 min, then for 2 h at 150 V in MOPS SDS running
549 buffer. Proteins were transferred onto 0.45 micron PVDF membrane in transfer buffer (50 mM
550 Tris, 192 mM Glycine and 0.05% SDS) containing 15% methanol with a Midi transfer apparatus
551 (Idea Scientific). Blots were blocked with 5 % non-fat dry milk in PBST (PBS with 0.05% Tween
552 20) or 1:10 Sea Block (Thermofisher, 37527). Blots were cut into pieces and incubated with rabbit
553 anti-SMC3 (Bethyl, A300-055A) at 1:1000 in block, rabbit anti-RAD21 (Bethyl, A300-080A,
554 BL331) at 1:1000, mouse anti-SA2 (Santa Cruz, J-12) at 1:1000, rabbit anti-CENPA (Millipore,
555 07-574) at 1:200 and rabbit anti-Histone H3 (Abcam, ab1791) at 1:10000 at 4°C overnight with
556 gentle rocking. Blots were washed 3 times with PBST then labeled with Horseradish Peroxidase
557 (HRP) conjugated goat anti-rabbit secondary (JacksonImmunoresearch, 11-035-144) at 1:20000.
558 For far red fluorescent detection, goat anti-rabbit, or anti-mouse (Azure biosystem, AC2128 and
559 AC2129) were used at 1:10000 at room temperature for 2.5 h. Blots were washed again 3 times
560 with PBST. For HRP detection blots were treated with Pierce West Pico reagent for 5 mins, then
561 captured by chemiluminescence with a Kodak 4000R Image Station. For far-red fluorescence,
562 membranes were imaged using an Azure c600 imaging system. Blot quantification was done
563 using the raw images with Metamorph Software (Molecular devices).
564 **Chromosome spreads:** Mitotic cells were washed with warm media by centrifuging at 300Xg for
565 3 min. Cells were suspended in 500 µl of warmed swelling buffer (40 % complete media + 60%
566 DI water). Samples were incubated in a 37°C water bath for 15-18 min. Swollen cells were fixed
567 by adding 1 ml 3:1 methanol: acetic acid, then incubated for 10 min. The cells were pelleted for 5
568 min at 250Xg, then washed with 1 ml fixative and pelleted once more. The cell pellets were
569 resuspended in 100-200 µl fixative, then 40-50 µl of cell suspension was dropped from a height
570 of 60 cm onto a 22 mm^2 coverslip that was cleaned with 95% ethanol and wiped with acetic acid.
571 The coverslips were immediately placed inside a 150 mm plastic culture dish on top of wet filter

572 paper. The lid was left off, and the coverslips were allowed to dry in the humidified chamber. Once
573 dried, coverslips were stained with DAPI (100 ng/ml) and SYBERGold nucleic acid dye (1:20000).
574 Slides were imaged with a Zeiss Axioplan II microscope using a 100X objective, Hamamatsu Orca
575 II camera and Metamorph software. At least 200 mitotic spreads were scored for each sample. If
576 an individual cell spread had more than 10 single chromatids, the cell was scored as fatigued.

577 **Live cell imaging:** Cells were grown in chambered cover glasses (Lab-Tek) for 24 h, then the
578 medium was changed to L-15 phenol red-free medium supplemented with P/S, NEAA and 10%
579 FBS. The surface of the medium was overlayered with mineral oil to reduce evaporation. For most
580 experiments, chambers were transferred to a Zeiss Axiovert microscope then imaged while using
581 an air-curtain heater to maintain the temperature at 37°C. Images were acquired every 7-10 min
582 for 18-20 h with a Zeiss 20X objective and ORCA-ER Hamamatsu camera using Metamorph
583 Software (Molecular Devices LLC). Images were analyzed using Metamorph software. For
584 experiments; Wapl depletion in SMC1-GFP cells, STLC treatment in HeLa-Fast, Taxol treatment
585 in HeLa-Slow, Rapamycin treatment in HeK293, ZM447439 treatment, and Sororin mutant
586 images were acquired using 20X objective in a Nikon Ti microscope fitted with an OKOlab
587 environmental chamber. For each cell that entered mitosis, the intervals from nuclear envelope
588 breakdown (NEBD) to metaphase and to anaphase onset or cohesion fatigue were recorded. To
589 induce metaphase arrest, cells were treated with 25 μM MG132 or 25 μM ProTAME, and scored
590 as fatigued when approximately 10% of the chromosomes had undergone chromatid separation.

591 For high resolution cohesion fatigue imaging, LLC-PK cells constitutively expressing EGFP-
592 Topoisomerase II alpha were grown on round 5mm glass coverslips in DMEM-based media to
593 densities between 60% and 80%. For control cultures exhibiting normal mitotic progression
594 DMSO was added to culture medium at 0.1%. To induce cohesion fatigue the 26S proteasome
595 inhibitor, MG132, dissolved in DMSO was added at 10 uM to experimental cultures which
596 resulted in a 0.1% DMSO concentration. Prior to image acquisition in order to improve

597 fluorescence capture and to remove the requirement for carbon dioxide pH buffering, media was
598 exchanged to phenol-free Leibovitz L-15 media with L-glutamine (Cat.# AT207-1L, VWR), 10 %
599 FBS, Penicillin, Streptomycin with or without MG132 as described above. Fluorescence images
600 of EGFP-Topoisomerase II alpha at 5 second intervals encompassing the entire cell volume
601 were acquired using the lattice light sheet microscope (LLSM) at Janelia Research Campus's
602 Advanced Imaging Center. Movies were prepared using Imaris software.

603 **siRNA experiments:** HeLa cells stably expressing SMC1-GFP were grown on chambered cover
604 glasses. Cells were transfected with Wapl siRNAs #1 GAGAGAUGUUUACGAGUUU; #2
605 CAACAGUGAAUCGAGUAA or universal negative control (Sigma catalog # SIC001) using RNAi
606 Max lipofectamine (Thermofisher catalog # 13778150). 48 h after transfection, live cell imaging
607 was done as described above. Only cells that showed a clear GFP signal on metaphase
608 chromosomes were included indicating significant depletion of Wapl. The elapsed time from
609 NEBD to metaphase and to chromatid separation was measured.

610 **Immunofluorescence:** Cells grown on 22 mm^2 coverslips were simultaneously fixed and
611 permeablized with 2% PFA and 0.5% Triton X-100 in 1X PHEM buffer at room temperature for 15
612 min. The cells were blocked with 20% boiled normal goat serum (BNGS) for at least 20 min.
613 Coverslips were incubated with primary antibody, CREST (1:800, Antibody INC, 15-134), rabbit
614 anti SGO1 (1:500, a gift from Dr. Hongtao Yu) diluted in 5% BNGS in PBST overnight at 4°C.
615 Coverslips were washed 3 times with MBST (MOPS buffered saline with 0.05% Tween 20), then
616 incubated in secondary antibody, goat anti-rabbit conjugated to CY3 at 1:1500 (JacksonImmuno,
617 111-165-045109) , goat anti-human conjugated to FITC at 1:800 (JacksonImmuno, 109-95-088)
618 for 2 h at room temperature. After incubation with secondary antibodies, coverslips were washed
619 three times again then labeled with DAPI (100 ng/ml) for one min. Coverslips were mounted on
620 slides with Vectashield mounting media (Victor labs, H-1000), then sealed with clear nail polish.
621 Fluorescence images of cells were taken using a Zeiss Axioplan II microscope with a Zeiss 100X

622 objective, Hamamatsu Orca II camera and Metamorph software. Distances between pairs of
623 kinetochores were measured using the region measurement tool in Metamorph software.

624 **Transient metaphase arrest:** For fixed cell analysis, LLC-PK cells grown on 22mm^2 were treated
625 with 5 μM MG132 ± 330 nM Nocodazole for 3 h. Arrested cells were washed 4 times with warm
626 DMEM then released into complete DMEM medium to complete mitosis. 3.5 h after release from
627 drug, cells were fixed with 3:1 methanol: acetic acid and labelled with (DAPI 100 ng/ml). Anaphase
628 cells were examined visually for lagging chromosomes or anaphase bridges with a Zeiss Axioplan
629 II and a Zeiss 100X objective. For identification of micronuclei, LLC-PK cells grown on coverslips
630 were transiently arrested with Nocodazole for 3 h or MG132 for 1 or 3 h then washed and released
631 into complete medium. 24 h after release, cells were fixed with 3:1 methanol: acetic acid then
632 labeled with DAPI (100 ng/ml). Each coverslip was imaged at 50 random positions with a Zeiss
633 Axiovert microscope and Zeiss 20X objective. The total number of cells and micronuclei in a field
634 was quantified using Metamorph software. For live cell imaging, HeLa-H2B-GFP cells grown on
635 chambered cover glasses were treated with 10, 20, or 30 μM ProTAME in L-15 medium then
636 imaged every 10 min for 18 h. Every cell that entered the mitosis was examined visually at
637 anaphase for any visible signs of anaphase bridges, lagging chromosomes or micronuclei
638 formation.

639

640

641 **Acknowledgements:**

642 We thank Dr. Arshad Desai for HeLa cells expressing H2B-mRFP, Dr. Kyoko Yokomori for HeLa
643 cells expressing SMC1-GFP, Dr. Todd Waldman for HCT116 SA2 knockout cells, Dr. Olaf
644 Stemmann for HeK293 cells expressing FRB- and FKBP-fused Cohesin proteins, and Dr.
645 Hongtao Yu for HeLa cell expressing 9A-mutnat Sororin and anti-SGO1 antibodies. We also thank
646 John Heddleston and Teng-Leong Chew at Janelia Research Campus's Advanced Imaging
647 Center and HHMI and More Foundation for providing instrumentation and technical assistance
648 for lattice light sheet microscopy imaging. Our thanks to all the members of Program in Cell Cycle
649 and Cancer Biology at OMRF for insightful discussion and comments. This work was supported
650 by the National Institute of General Medical Sciences (R01GM111731) and by the McCasland
651 Foundation.

652 **References**

653 Bermudez, V.P., A. Farina, T.L. Higashi, F. Du, I. Tappin, T.S. Takahashi, and J. Hurwitz. 2012.
654 In vitro loading of human cohesin on DNA by the human Scc2-Scc4 loader complex.
655 *Proc Natl Acad Sci U S A*. 109:9366-9371.
656 Brinkley, B.R., R.P. Zinkowski, W.L. Mollon, F.M. Davis, M.A. Pisegna, M. Pershouse, and P.N.
657 Rao. 1988. Movement and segregation of kinetochores experimentally detached from
658 mammalian chromosomes. *Nature*. 336:251-254.
659 Buheitel, J., and O. Stemmann. 2013. Prophase pathway-dependent removal of cohesin from
660 human chromosomes requires opening of the Smc3-Scc1 gate. *Embo j*. 32:666-676.
661 Canudas, S., and S. Smith. 2009. Differential regulation of telomere and centromere cohesion
662 by the Scc3 homologues SA1 and SA2, respectively, in human cells. *J Cell Biol*.
663 187:165-173.
664 Cimini, D., B. Moree, J.C. Canman, and E.D. Salmon. 2003. Merotelic kinetochore orientation
665 occurs frequently during early mitosis in mammalian tissue cells and error correction is
666 achieved by two different mechanisms. *J Cell Sci*. 116:4213-4225.
667 Crasta, K., N.J. Ganem, R. Dagher, A.B. Lantermann, E.V. Ivanova, Y. Pan, L. Nezi, A.
668 Protopopov, D. Chowdhury, and D. Pellman. 2012. DNA breaks and chromosome
669 pulverization from errors in mitosis. *Nature*. 482:53-58.
670 Daum, J.R., T.A. Potapova, S. Sivakumar, J.J. Daniel, J.N. Flynn, S. Rankin, and G.J. Gorbsky.
671 2011. Cohesion fatigue induces chromatid separation in cells delayed at metaphase.
672 *Curr Biol*. 21:1018-1024.
673 Ertych, N., A. Stolz, A. Stenzinger, W. Weichert, S. Kaulfuss, P. Burfeind, A. Aigner, L.
674 Wordeman, and H. Bastians. 2014. Increased microtubule assembly rates influence
675 chromosomal instability in colorectal cancer cells. *Nat Cell Biol*. 16:779-791.
676 Gandhi, R., P.J. Gillespie, and T. Hirano. 2006. Human Wapl is a cohesin-binding protein that
677 promotes sister-chromatid resolution in mitotic prophase. *Curr Biol*. 16:2406-2417.
678 Haarhuis, J.H., A.M. Elbatsh, B. van den Broek, D. Camps, H. Erkan, K. Jalink, R.H. Medema,
679 and B.D. Rowland. 2013. WAPL-mediated removal of cohesin protects against
680 segregation errors and aneuploidy. *Curr Biol*. 23:2071-2077.
681 Haarhuis, J.H.I., R.H. van der Weide, V.A. Blomen, J.O. Yanez-Cuna, M. Amendola, M.S. van
682 Ruiten, P.H.L. Krijger, H. Teunissen, R.H. Medema, B. van Steensel, T.R.
683 Brummelkamp, E. de Wit, and B.D. Rowland. 2017. The Cohesin Release Factor WAPL
684 Restricts Chromatin Loop Extension. *Cell*. 169:693-707.e614.
685 Hatch, E.M., A.H. Fischer, T.J. Deerinck, and M.W. Hetzer. 2013. Catastrophic nuclear
686 envelope collapse in cancer cell micronuclei. *Cell*. 154:47-60.
687 Hauf, S., E. Roitinger, B. Koch, C.M. Dittrich, K. Mechtler, and J.M. Peters. 2005. Dissociation of
688 cohesin from chromosome arms and loss of arm cohesion during early mitosis depends
689 on phosphorylation of SA2. *PLoS Biol*. 3:e69.
690 Hou, F., C.W. Chu, X. Kong, K. Yokomori, and H. Zou. 2007. The acetyltransferase activity of
691 San stabilizes the mitotic cohesin at the centromeres in a shugoshin-independent
692 manner. *J Cell Biol*. 177:587-597.
693 Kleyman, M., L. Kabeche, and D.A. Compton. 2014. STAG2 promotes error correction in mitosis
694 by regulating kinetochore-microtubule attachments. *J Cell Sci*. 127:4225-4233.
695 Kueng, S., B. Hegemann, B.H. Peters, J.J. Lipp, A. Schleiffer, K. Mechtler, and J.M. Peters.
696 2006. Wapl controls the dynamic association of cohesin with chromatin. *Cell*. 127:955-
697 967.
698 Lara-Gonzalez, P., and S.S. Taylor. 2012. Cohesion fatigue explains why pharmacological
699 inhibition of the APC/C induces a spindle checkpoint-dependent mitotic arrest. *PLoS*
700 *One*. 7:e49041.

701 Liu, H., L. Jia, and H. Yu. 2013a. Phospho-H2A and cohesin specify distinct tension-regulated
702 Sgo1 pools at kinetochores and inner centromeres. *Curr Biol*. 23:1927-1933.
703 Liu, H., S. Rankin, and H. Yu. 2013b. Phosphorylation-enabled binding of SGO1-PP2A to
704 cohesin protects sororin and centromeric cohesion during mitosis. *Nat Cell Biol*. 15:40-
705 49.
706 McGuinness, B.E., T. Hirota, N.R. Kudo, J.M. Peters, and K. Nasmyth. 2005. Shugoshin
707 prevents dissociation of cohesin from centromeres during mitosis in vertebrate cells.
708 *PLoS Biol*. 3:e86.
709 Michaelis, C., R. Ciosk, and K. Nasmyth. 1997. Cohesins: chromosomal proteins that prevent
710 premature separation of sister chromatids. *Cell*. 91:35-45.
711 Murayama, Y., and F. Uhlmann. 2015. DNA Entry into and Exit out of the Cohesin Ring by an
712 Interlocking Gate Mechanism. *Cell*. 163:1628-1640.
713 Nishiyama, T., R. Ladurner, J. Schmitz, E. Kreidl, A. Schleiffer, V. Bhaskara, M. Bando, K.
714 Shirahige, A.A. Hyman, K. Mechtler, and J.M. Peters. 2010. Sororin mediates sister
715 chromatid cohesion by antagonizing Wapl. *Cell*. 143:737-749.
716 Nishiyama, T., M.M. Sykora, P.J. Huis in 't Veld, K. Mechtler, and J.M. Peters. 2013. Aurora B
717 and Cdk1 mediate Wapl activation and release of acetylated cohesin from chromosomes
718 by phosphorylating Sororin. *Proc Natl Acad Sci U S A*. 110:13404-13409.
719 Ocampo-Hafalla, M.T., Y. Katou, K. Shirahige, and F. Uhlmann. 2007. Displacement and re-
720 accumulation of centromeric cohesin during transient pre-anaphase centromere splitting.
721 *Chromosoma*. 116:531-544.
722 Sackton, K.L., N. Dimova, X. Zeng, W. Tian, M. Zhang, T.B. Sackton, J. Meaders, K.L. Pfaff, F.
723 Sigoillot, H. Yu, X. Luo, and R.W. King. 2014. Synergistic blockade of mitotic exit by two
724 chemical inhibitors of the APC/C. *Nature*. 514:646-649.
725 Salmon, E.D., D. Cimini, L.A. Cameron, and J.G. DeLuca. 2005. Merotelic kinetochores in
726 mammalian tissue cells. *Philos Trans R Soc Lond B Biol Sci*. 360:553-568.
727 Shintomi, K., and T. Hirano. 2009. Releasing cohesin from chromosome arms in early mitosis:
728 opposing actions of Wapl-Pds5 and Sgo1. *Genes Dev*. 23:2224-2236.
729 Skibbens, R.V. 2016. Of Rings and Rods: Regulating Cohesin Entrapment of DNA to Generate
730 Intra- and Intermolecular Tethers. *PLoS Genet*. 12:e1006337.
731 Skoufias, D.A., S. DeBonis, Y. Saoudi, L. Lebeau, I. Crevel, R. Cross, R.H. Wade, D. Hackney,
732 and F. Kozielski. 2006. S-trityl-L-cysteine is a reversible, tight binding inhibitor of the
733 human kinesin Eg5 that specifically blocks mitotic progression. *J Biol Chem*. 281:17559-
734 17569.
735 Solomon, D.A., T. Kim, L.A. Diaz-Martinez, J. Fair, A.G. Elkahloun, B.T. Harris, J.A. Toretsky,
736 S.A. Rosenberg, N. Shukla, M. Ladanyi, Y. Samuels, C.D. James, H. Yu, J.S. Kim, and
737 T. Waldman. 2011. Mutational inactivation of STAG2 causes aneuploidy in human
738 cancer. *Science*. 333:1039-1043.
739 Stevens, D., R. Gassmann, K. Oegema, and A. Desai. 2011. Uncoordinated loss of chromatid
740 cohesion is a common outcome of extended metaphase arrest. *PLoS One*. 6:e22969.
741 Sumara, I., E. Vorlaufer, C. Gieffers, B.H. Peters, and J.M. Peters. 2000. Characterization of
742 vertebrate cohesin complexes and their regulation in prophase. *J Cell Biol*. 151:749-762.
743 Tanno, Y., H. Susumu, M. Kawamura, H. Sugimura, T. Honda, and Y. Watanabe. 2015. The
744 inner centromere-shugoshin network prevents chromosomal instability. *Science*.
745 349:1237-1240.
746 Tedeschi, A., G. Wutz, S. Huet, M. Jaritz, A. Wuensche, E. Schirghuber, I.F. Davidson, W.
747 Tang, D.A. Cisneros, V. Bhaskara, T. Nishiyama, A. Vaziri, A. Wutz, J. Ellenberg, and
748 J.M. Peters. 2013. Wapl is an essential regulator of chromatin structure and
749 chromosome segregation. *Nature*. 501:564-568.

750 Thompson, S.L., and D.A. Compton. 2011. Chromosome missegregation in human cells arises
751 through specific types of kinetochore-microtubule attachment errors. *Proc Natl Acad Sci*
752 *U S A*. 108:17974-17978.
753 Tomonaga, T., K. Nagao, Y. Kawasaki, K. Furuya, A. Murakami, J. Morishita, T. Yuasa, T.
754 Sutani, S.E. Kearsey, F. Uhlmann, K. Nasmyth, and M. Yanagida. 2000.
755 Characterization of fission yeast cohesin: essential anaphase proteolysis of Rad21
756 phosphorylated in the S phase. *Genes Dev*. 14:2757-2770.
757 Uhlmann, F., D. Wernic, M.A. Poupart, E.V. Koonin, and K. Nasmyth. 2000. Cleavage of
758 cohesin by the CD clan protease separin triggers anaphase in yeast. *Cell*. 103:375-386.
759 Unal, E., A. Arbel-Eden, U. Sattler, R. Shroff, M. Lichten, J.E. Haber, and D. Koshland. 2004.
760 DNA damage response pathway uses histone modification to assemble a double-strand
761 break-specific cohesin domain. *Mol Cell*. 16:991-1002.
762 Vallot, A., I. Leontiou, D. Cladiere, W. El Yakoubi, S. Bolte, E. Buffin, and K. Wassmann. 2017.
763 Tension-Induced Error Correction and Not Kinetochore Attachment Status Activates the
764 SAC in an Aurora-B/C-Dependent Manner in Oocytes. *Curr Biol*.
765 van der Lelij, P., S. Lieb, J. Jude, G. Wutz, C.P. Santos, K. Falkenberg, A. Schlattl, J. Ban, R.
766 Schwentner, T. Hoffmann, H. Kovar, F.X. Real, T. Waldman, M.A. Pearson, N. Kraut,
767 J.M. Peters, J. Zuber, and M. Petronczki. 2017. Synthetic lethality between the cohesin
768 subunits STAG1 and STAG2 in diverse cancer contexts. *Elife*. 6.
769 Waizenegger, I.C., S. Hauf, A. Meinke, and J.-M. Peters. 2000. Two Distinct Pathways Remove
770 Mammalian Cohesin from Chromosome Arms in Prophase and from Centromeres in
771 Anaphase. *Cell*. 103:399-410.
772 Whelan, G., E. Kreidl, G. Wutz, A. Egner, J.M. Peters, and G. Eichele. 2012. Cohesin
773 acetyltransferase Esco2 is a cell viability factor and is required for cohesion in pericentric
774 heterochromatin. *Embo j*. 31:71-82.
775 Xu, B., S. Lu, and J.L. Gerton. 2014. Roberts syndrome: A deficit in acetylated cohesin leads to
776 nucleolar dysfunction. *Rare Dis*. 2:e27743.
777 Xu, X., R. Kanai, N. Nakazawa, L. Wang, C. Toyoshima, and M. Yanagida. 2018. Suppressor
778 mutation analysis combined with 3D modeling explains cohesin's capacity to hold and
779 release DNA. *Proc Natl Acad Sci U S A*.
780 Xu, Z., B. Cetin, M. Anger, U.S. Cho, W. Helmhart, K. Nasmyth, and W. Xu. 2009. Structure and
781 function of the PP2A-shugoshin interaction. *Mol Cell*. 35:426-441.
782 Yeh, E., J. Haase, L.V. Paliulis, A. Joglekar, L. Bond, D. Bouck, E.D. Salmon, and K.S. Bloom.
783 2008. Pericentric chromatin is organized into an intramolecular loop in mitosis. *Curr Biol*.
784 18:81-90.
785 Zeng, X., F. Sigoillot, S. Gaur, S. Choi, K.L. Pfaff, D.C. Oh, N. Hathaway, N. Dimova, G.D.
786 Cuny, and R.W. King. 2010. Pharmacologic inhibition of the anaphase-promoting
787 complex induces a spindle checkpoint-dependent mitotic arrest in the absence of spindle
788 damage. *Cancer Cell*. 18:382-395.
789 Zhang, C.Z., A. Spektor, H. Cornils, J.M. Francis, E.K. Jackson, S. Liu, M. Meyerson, and D.
790 Pellman. 2015. Chromothripsis from DNA damage in micronuclei. *Nature*. 522:179-184.
791 Zhang, N., S.G. Kuznetsov, S.K. Sharan, K. Li, P.H. Rao, and D. Pati. 2008. A handcuff model
792 for the cohesin complex. *J Cell Biol*. 183:1019-1031.

793

794 **Figure Legends**

795 **Figure 1: The core Cohesin protein SMC3 remains bound to chromatids during cohesion**
796 **fatigue.**

797 **(A)** Immunoblotting of chromosome fractions from mitotic HeLa cells treated with MG132
798 ±Nocodazole for 8 h. Lane 1 shows baseline salt-resistant SMC3 level in mitotic chromosomes
799 before cohesion fatigue. Lane 2 reflects SMC3 in chromosome fractions of fatigued chromatids.
800 Lane 3 shows SMC3 in negative control for cohesion fatigue (MG132 +Nocodazole). **(B)**
801 Quantified immunoblots from four independent experiments where band intensity of SMC3 was
802 measured and normalized to CENP-A band intensity. Dotted line on graph represents the
803 expected level of SMC3 if cohesin was lost from fatigued chromosomes based on the percentage
804 of separated chromosomes seen in chromosome spreads. Kruskal-Wallis test with Dunn's
805 multiple comparison was used for statistical analysis. Error bars represent standard deviation.

806 **Figure 2: Wapl-mediated release of Cohesin after metaphase is not required for cohesion**
807 **fatigue.**

808 **(A)** Wapl depletion during interphase slows cohesion fatigue in subsequent mitosis. Elapsed times
809 from metaphase to chromatid separation/cohesion fatigue were determined via live cell imaging
810 in HeLa cells stably expressing SMC1-GFP. In Wapl-depleted cells, only cells with clear GFP
811 signal on chromosomes at the metaphase plate (indicating successful Wapl depletion) were
812 scored in two independent experiments with totals of >100 cells. **(B)** Expression of
813 phosphorylation resistant Sororin slows cohesion fatigue. Elapsed times from metaphase to
814 cohesion fatigue were determined in HeLa cells expressing either WT sororin or non-
815 phosphorylatable 9A-sororin. At least 60 cells were scored for each cell type. The Mann-Whitney
816 test was used for statistical analysis. **(C)** Inhibition of Aurora B kinase after metaphase alignment
817 does not inhibit cohesion fatigue. Experimental scheme and graph depicting elapsed times from

818 metaphase to cohesion fatigue were determined after 2.5 uM ZM 447439 treatment in cells
819 released from Nocodazole to MG132 for 1 h. Three independent experiments with totals of >200
820 cells were quantified. The Mann-Whitney test was used for statistical analysis. **(D)** Locking the
821 SMC3-Rad21 gate but not other gates before mitotic entry inhibits cohesion fatigue. Experimental
822 scheme and results from chromosome spreads in Hek293 expressing Cohesin fusions to
823 Rapamycin-binding proteins treated with Rapamycin to lock specific gates **before cells entered**
824 **mitosis** then treated with MG132 for 6 h to arrest cells at metaphase and allow cohesion fatigue.
825 Totals of >100 spreads per condition per cell line were quantified. Graph shows mean±S.E.M.
826 Dotted line represents the expected inhibition of fatigue with efficient SMC3-RAD21 gate locking
827 based on % of spreads with unresolved chromatid arms (45%) from supplementary figure 2D. **(E)**
828 Locking any of the Cohesin gates after completion of Wapl-mediated Cohesin release in early
829 mitosis does not inhibit cohesion fatigue. HEK293 cells expressing Cohesin fusions to
830 Rapamycin-binding proteins were treated with or without Rapamycin **after allowing completion**
831 **of early mitosis, Wapl-mediated Cohesin removal** in three independent experiments with totals
832 of > 450 spreads per cells line for each treatment. Graph shows Mean±S.D. Two-way ANOVA
833 with Tukey's multiple comparison test was used for statistical analysis.

834 **Figure 3**: **Altering Cohesin changes the rate of cohesion fatigue.**

835 **(A)** Longer mitotic arrest in Nocodazole leads to enhanced cohesion fatigue. Experimental
836 scheme and chromosome spread analysis for LLC-PK cells arrested in mitosis for 5 or 11 h with
837 330 nM Nocodazole, then washed and treated with MG132 ±Nocodazole (330 nM) to arrest at
838 metaphase for 3 or 6 h. Three independent experiments with a total of >600 spreads were scored
839 for each treatment. Cells initially arrested for 11 h in Nocodazole undergo more rapid cohesion
840 fatigue than those arrested for 5 h, consistent with the continued action of the Wapl-mediated
841 prophase pathway in removing Cohesin from chromosomes in cells arrested in mitosis. Error bars
842 show standard deviation. Two-way ANOVA with Sidak's multiple test was used for statistical

843 analysis. **(B)** SA2 knockout HCT116 cells undergo cohesion fatigue more rapidly than parental
844 cells. Chromosome spreads were examined in parental and SA2 knockout HCT116 cells. Cells
845 were treated with 330 nM Nocodazole overnight (16 h), then mitotic cells were collected, washed
846 then treated with MG132 ±Nocodazole (330 nM) for 3 or 6 h. Three independent experiments with
847 totals of >600 spreads were scored. Two-way ANOVA with Sidak's multiple test was used for
848 statistical analysis. **(C)** SA2 protein is not lost from chromatids during cohesion fatigue.
849 Immunoblotting of SA2 protein in chromosome fractions prepared from mitotic HeLa cells treated
850 with MG132 ±Nocodazole for 8 h. Lane 1 shows baseline SA2 levels in mitotic chromosomes,
851 lane 2 shows SA2 in chromosome fractions from fatigued chromatids and lane 3 shows cohesion
852 fatigue negative control (MG132 plus 330 nM Nocodazole for 8 h).

853 **Figure 4: Microtubule dynamics and spindle tension impact cohesion fatigue.**

854 **(A)** Treatment of cells with low concentration of Nocodazole slows cohesion fatigue. The elapsed
855 time from metaphase to chromatid scattering/cohesion fatigue was determined in HeLa-Slow cells
856 (left) and HeLa-Fast cells (right) arrested at metaphase with MG132 +/- 5nM Nocodazole **(B)**
857 Treatment of cells with low concentration of Taxol accelerates cohesion fatigue. The elapsed time
858 from metaphase to chromatid scattering/cohesion fatigue was determined in HeLa-Slow cells (left)
859 and HeLa-Fast cells (right) arrested at metaphase with ProTAME +/- 1.5nM Taxol. **(C)**
860 Decreasing spindle tension with low concentration of STLC slows cohesion fatigue. The elapsed
861 time from metaphase to chromatid scattering/cohesion fatigue was determined in HeLa-Slow cells
862 (left) and HeLa-Fast cells (right) arrested at metaphase with ProTAME +/- 1.5μM STLC. Three
863 independent experiments with a total of ≥150 cells were scored for each treatment and cell type.
864 Error bars show standard deviation. The Mann-Whitney test was used for statistical analysis.

865

866 **Figure 5: Separated chromatids can congress to the spindle midplane after cohesion**
867 **fatigue.**

868 (**A)** Cohesion fatigue was assessed in HeLa cells stably expressing H2B-GFP treated with either
869 DMSO (control) or ProTAME via live cell imaging. Time 00 indicates nuclear envelop breakdown
870 (NEBD). DMSO-treated cells progress through normal mitosis (top panel), while ProTAME-treated
871 cells undergo cohesion fatigue with a concentration of chromatin at the spindle midplane in the
872 final image (bottom panel). **(B)** Chromosome spreads prepared from HeLa cells treated with
873 MG132 ±Nocodazole for 8 h. Left panel shows paired sister chromatids (MG132+Nocodazole).
874 Right panel shows separated sister chromatids (cohesion fatigue) after 8 h of metaphase arrest
875 (MG132).

876 **Figure 6: Sister kinetochores separate after transient metaphase arrest.**

877 **(A)** Transient metaphase arrest results in increased separation of sister kinetochores in LLC-PK
878 cells. Representative immunofluorescence images (left) and quantification (right) of control
879 metaphase cells or cells arrested at metaphase for up to 1 h and up to 2-3 h. The average
880 distances between pairs of kinetochores from were compared in control metaphase cells and cells
881 treated with MG132 for 1 or 3 h (n ≥ 125 kinetochore pairs in 5 cells from each treatment). One-
882 way ANOVA, with Tukey's multiple comparison test was used for statistical analysis. **(B**) The
883 frequency distributions for distances between sister kinetochores from cells in (A) show increased
884 proportions widely separated kinetochores in those arrested for 3 h. **(C)** The extent of stretching
885 between sister kinetochores increases with time for cells arrested at metaphase. Live cell imaging
886 determined the maximum stretching of sister kinetochores in LLC-PK cells arrested at metaphase
887 for 1 or 2-3 h. For these measurements, n ≥ 10 pairs of kinetochores were imaged every 10 sec
888 for 3 min. Kruskal-Wallis test with Dunn's multiple comparison was used for statistical analysis.

889 **Figure 7: Transient metaphase delays induce segregation defects in LLC-PK cells.**

890 **(A)** Representative images (left) and quantification (right) of anaphase/telophase segregation
891 defects (lagging chromosomes, anaphase bridges, or micronuclei) in LLC-PK cells transiently
892 arrested at metaphase. Segregation defects during anaphase were examined in untreated cells
893 or in cells transiently treated with Nocodazole, MG132, or MG132 +Nocodazole for 3 h in three
894 independent experiments with >700 anaphases examined for each treatment. Error bars
895 represent standard deviations. Ordinary one-way ANOVA with Holm-Sidak's multiple comparison
896 test was used for statistical analysis. **(B)** Transient delays at metaphase induce formation of
897 persistent micronuclei. Low magnification images of LLC-PK cells transiently arrested at a
898 prometaphase-like state with nocodazole or at metaphase with MG132 for 3 h then released for
899 24 h. Arrows indicate the micronuclei present in cells that were transiently delayed at metaphase.
900 **(C)** Percentages of micronuclei in images from (B) were determined in ≥5000 cells from 50
901 randomly selected fields. One-way ANOVA was used for statistical analysis.

902 **Figure 8: Segregation defects in HeLa cells scale with the length of metaphase delay.**

903 **(A)** Live-cell images of HeLa-H2B-GFP cells treated with 10, 20 or 30 μM ProTAME. Top panel
904 shows a normal anaphase; bottom two panel show anaphase defects (arrows indicate
905 micronuclei). **(B)** Fates of individual cells after ProTAME treatment. Most cells with slight delays
906 had no segregation defects; intermediate delays increased the proportion of defective anaphase,
907 while longer delays often resulted in cohesion fatigue. **(C)** Compiling of results for cells treated
908 with ProTAME shows the increased anaphase defects at intermediate times of metaphase delay
909 and increased cohesion fatigue at longer times.

910 **Supplemental Figure Legends**

911 **Supplemental figure 1: Buffers containing moderate levels of salt removes most Cohesin**
912 **from isolated mitotic chromosomes, and Sgo1 levels do not correlate with cohesion**
913 **fatigue.**

914 **(A)** Titration of Cohesin SMC3 and CENP-A used for quantification of Cohesin proteins. Dilutions
915 of the 0 h sample were blotted with samples from other treatments and time points. The linear
916 ranges of dilutions were determined for accurate quantification of the Cohesin component SMC3
917 (top) and loading control CENP-A (bottom). The vertical dotted lines represent the number of cells
918 that generate linear protein loaded to signal ratios. 10000 cells equivalent protein was loaded for
919 subsequent experiments. **(B)** Immunoblot of Cohesin components (SMC3 and RAD21) from
920 chromosome/chromatin fractions of mitotic and interphase (G2) HeLa cells isolated in buffers with
921 increasing NaCl. Cohesin was readily released from mitotic chromosomes compared to
922 interphase chromatin by salt treatment. More than 90% of Cohesin was released from mitotic
923 chromosomes by treatment with 100 mM NaCl. **(C)** Total SGO1 levels relative to CREST signals
924 were determined by immunofluorescence in HeLa-Slow and HeLa-Fast cells. At least 10 cells for
925 each cell line were quantified. **(D)** SGO1 levels determined by immunofluorescence in HeLa-Slow
926 cells that were treated with MG132 for 6h. **(E)** Total SGO1 levels in HeLa-Fast cells treated with
927 MG132 for 3h. For each cell line and treatment, at least 5 randomly selected cells were imaged
928 with 0.5 μm Z sections. Summed projections were generated with Metamorph Software using the
929 stack arithmetic tool. Region of DAPI staining was used as the mask to quantify total
930 chromosome-associated SGO1.

931

932 **Supplemental figure 2: Inhibition of the prophase pathway before mitotic entry enriches**
933 **chromosome-bound Cohesin and delays cohesion fatigue.**

934 **(A)** Images from live cell imaging of HeLa-SMC1-GFP cells depleted of Wapl by RNAi. Wapl-
935 depletion resulted in cells showing strong SMC1-GFP signals on mitotic chromosomes. **(B)** The
936 elapsed times from NEBD to metaphase were determined in Hells treated with 0.5 uM ZM447439.
937 ZM Treatment caused significant delays in chromosome alignment indicating Aurora B inhibition.
938 >100 cells for each treatment were scored. **(C)** Chromosome spread on the left shows unresolved
939 chromosome arms in a cell where the Wapl-mediated cohesin release was blocked by locking
940 SMC3-RAD21 interface prior to entrance of cells into mitosis. Spread on right is from a control
941 cell of the same type without Rapamycin addition (unlocked SMC3-RAD21 gate). **(D)** Percentages
942 of chromosome spreads with closed/unresolved chromosome arms in HEK293 cells expressing
943 pairs of Cohesin fusions to which Rapamycin was added to lock different Cohesin gates.
944 Unresolved arms were increased only when the SMC-RAD21 gate was locked. **(E)** Elapsed times
945 form metaphase to cohesion fatigue were determined in three gate-locking Hek293 cells line with
946 gates locked prior to mitotic entry. Locking the SMC3-RAD21 gate but not other gates delayed
947 cohesion fatigue.

948 **Supplemental figure 3: Longer mitotic arrest reduces the levels of chromosome Cohesin**
949 **and the amount of chromosome-associated Cohesin is reduced in cells lacing SA2.**

950 **(A)** Longer mitotic arrest in Nocodazole results in greater separation of chromosome arms. Cells
951 were arrested with Nocodazole for 3 h (left panel) or 14 h (right panel) then prepared for
952 chromosome spreads. **(B)** Cells that take longer to align their chromosomes fatigue faster.
953 Elapsed times from metaphase to cohesion fatigue in STLC+ProTAME-treated cells plotted
954 against times from NEBD to metaphase. **(C)** A small reduction of salt-resistant SMC3 in
955 chromosome fractions accompanies longer arrest in Nocodazole. Immunoblot of chromosome
956 fractions from mitotic HeLa cells arrested in mitosis with Nocodazole for 5h or 11h. Graph shows

957 quantification. **(D)** SA2 knockout HCT116 cells lack expression of detectable SA2 protein.
958 Immunoblot with anti-SA2 antibody of whole cell lysates of SA2 knockout HCT116 cells and
959 parental HCT116 cells. **(E)** Core Cohesin ring protein levels are reduced in SA2 knockout cells
960 relative to parental cells. Immunoblot of salt-treated chromosome fractions from HCT116 SA2
961 knockout and parental cells. Graph shows band intensity of SMC3 and RAD21 relative to CENP-
962 A.

963 **Supplemental figure 4: HeLa-Fast and HeLa–Slow cells differ in fatigue kinetics, and HeLa-**
964 **Slow cells undergo slower mitosis in low concentrations of spindle drugs.**

965 **(A)** The elapsed time from metaphase to chromatid separation (cohesion fatigue) was determined
966 from live cell imaging in HeLa-Slow and HeLa-Fast cells treated with 25 uM ProTAME. Average
967 times of fatigue with standard deviations are shown from three independent experiments with
968 ≥300 cells. Mann-Whitney test was used for statistical analysis. **(B)** Kinetics of cohesion fatigue
969 in cells from (A). **(C)** HeLa-Slow cells treated with low concentrations of Nocodazole (5 nM) or
970 Taxol (1.5 nM) show slowed progression through mitosis. The elapsed times from NEBD to
971 anaphase was determined by live cell imaging. **(D)** Low concentration of STLC slowed but did not
972 block mitotic progression in HeLa-Slow cells. The elapsed time from NEBD to anaphase was
973 determined with cells treated with 1.5 μM STLC with ≥100 cells per treatment scored.

974 **Supplemental figure 5: Short metaphase arrest causes increased interkinetochore**
975 **distance only in the presence of a functional spindle.**

976 **(A)** Interkinetochore distances were measured in LLC-PK cells treated with MG132 and
977 Nocodazole for 1 or 3 h compared to normal metaphase (Control). A total of ≥100 kinetochore
978 pairs from 5 cells were measured. One-way ANOVA was used for statistical analysis. **(B)**
979 Interkinetochore distances were measured in HeLa cells arrested at metaphase with MG132 for
980 30 min or 3 h. A total of ≥100 kinetochore pairs from 5 cells were measured. **(C)** Interkinetochore

981 distances were determined from live cell imaging in LLC-PK cells stably expressing Topo-II-GFP.
982 Cells were arrested in metaphase with MG132 treatment for 1 or 3 h. Transient metaphase arrest
983 led to significant kinetochore separation if spindle microtubules were intact.

984 **Supplemental figure 6: MG132 and ProTAME induce metaphase delays whose duration**
985 **determines cell fate.**

986 **(A)** Percentages of defective anaphases in LLC-PK cells treated with MG132 for 1 or 4 h then
987 released into drug-free medium. **(B)** Metaphase arrest durations were determined from live cell
988 imaging of HeLa-Slow cells treated with increasing concentrations of ProTAME. For each
989 concentration of ProTAME, ≥75 cells were scored. The Kruskal-Wallis test was used for statistical
990 analysis. **(C)** The average length of metaphase arrest was determined in cells from (B) that exited
991 mitosis to 1) normal anaphase, 2) defective anaphase, or 3) cohesion fatigue.

992

993 **Supplemental Videos**

994 **Supplemental Video 1:** Normal mitotic progression visualized by lattice light sheet microscopy
995 in LLC-PK cells stably expressing EGFP-Topoisomerase IIα, which highlights kinetochores and
996 chromosome arms. Time = min:sec.

997 **Supplemental Video 2:** Consequences of cohesion fatigue visualized by lattice light sheet
998 microscopy in LLC-PK cells stably expressing EGFP-Topoisomerase IIα. Imaging was initiated 6
999 h after metaphase arrest induced by treatment with MG132. Some chromatids (00 min, middle
1000 left) have separated completely. Other chromosomes show extensive separation of their
1001 kinetochores but retain partially cohered arms. Separated kinetochores undergo oscillations
1002 toward and away from the spindle equator. Time = min:sec

figure_1

A

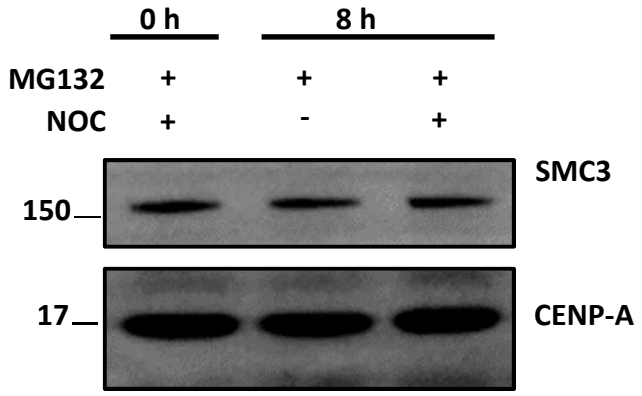
0 h
8 h
MG132 + + +
NOC + - +
150
SMC3
17
CENP-A

B

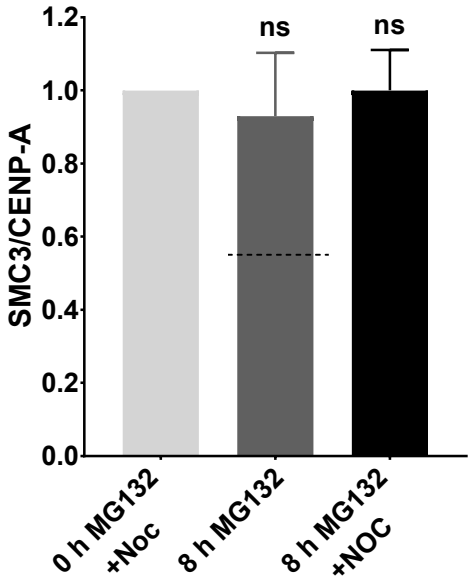
SMC3/CENP-A
1.2
1.0
0.8
0.6
0.4
0.2
0.0
ns
ns
0 h MG132 +Noc
8 h MG132
8 h MG132 +NOC

Figure_2

A

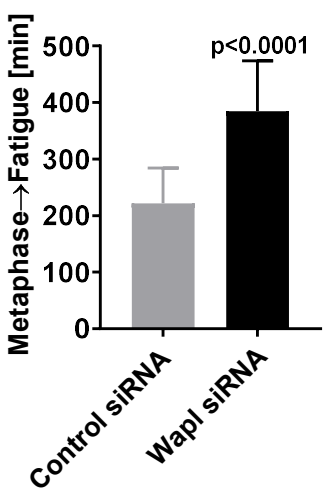

B

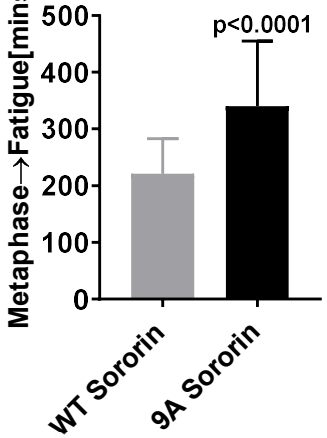

C

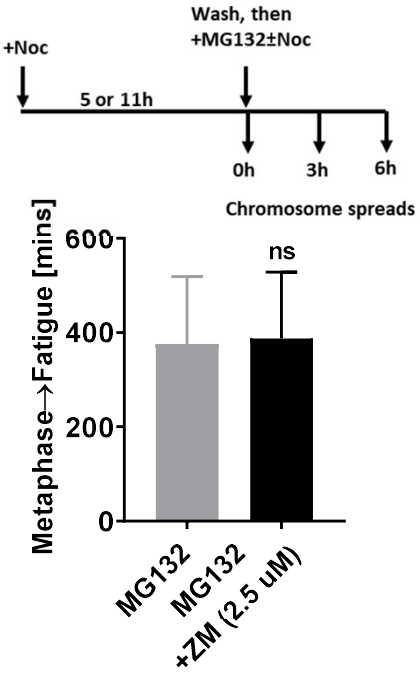

D Gates locked **before** Wapl-mediated cohesin removal

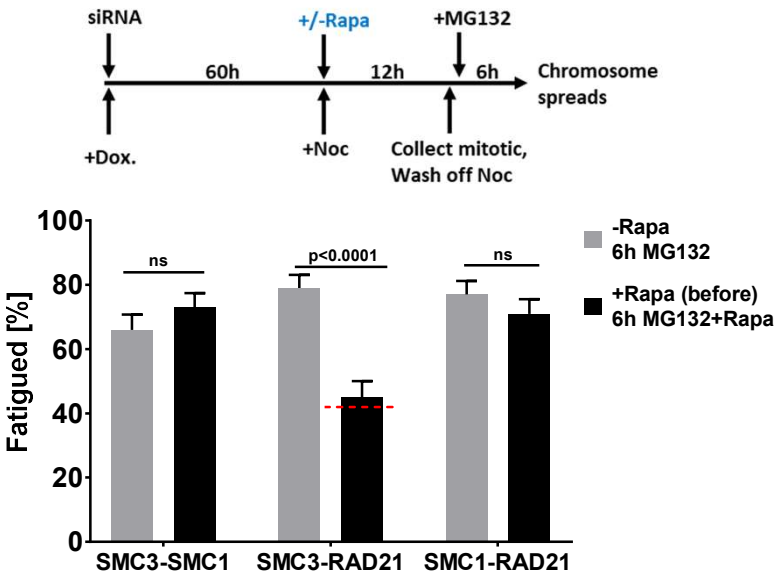

E Gates locked **after** Wapl-mediated cohesin removal

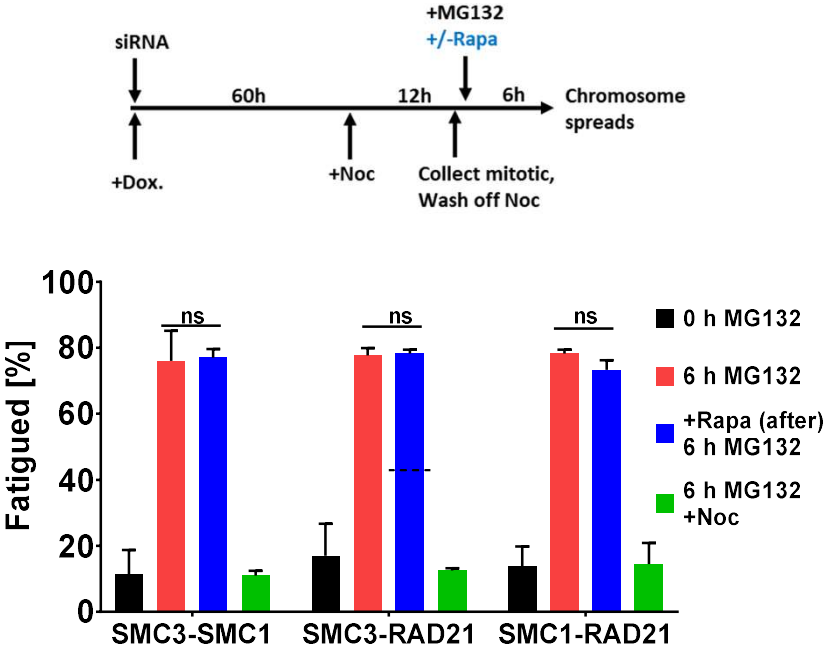

figure_3

A

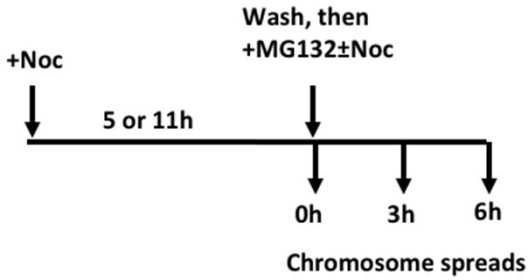
+Noc
5 or 11h
Wash, then
+MG132±Noc
0h
3h
6h
Chromosome spreads

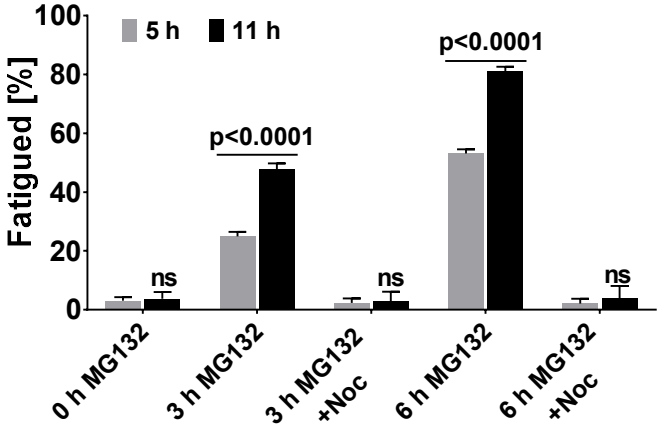
5 h
11 h
Fatigued [%]
100
80
60
40
20
0
p<0.0001
p<0.0001
ns
ns
ns
0 h MG132
3 h MG132
3 h MG132 +Noc
6 h MG132
6 h MG132 +Noc

B

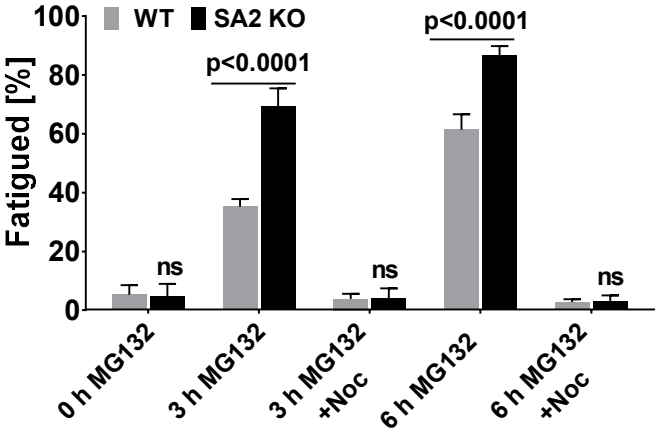
WT
SA2 KO
Fatigued [%]
100
80
60
40
20
0
p<0.0001
p<0.0001
ns
ns
ns
0 h MG132
3 h MG132
3 h MG132 +Noc
6 h MG132
6 h MG132 +Noc

C

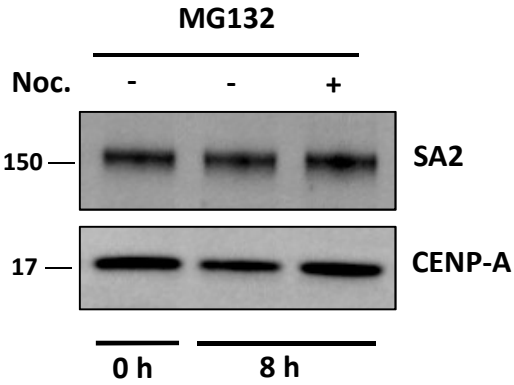
MG132
Noc.
-
-
+
150
SA2
17
CENP-A
0 h
8 h

Figure_4

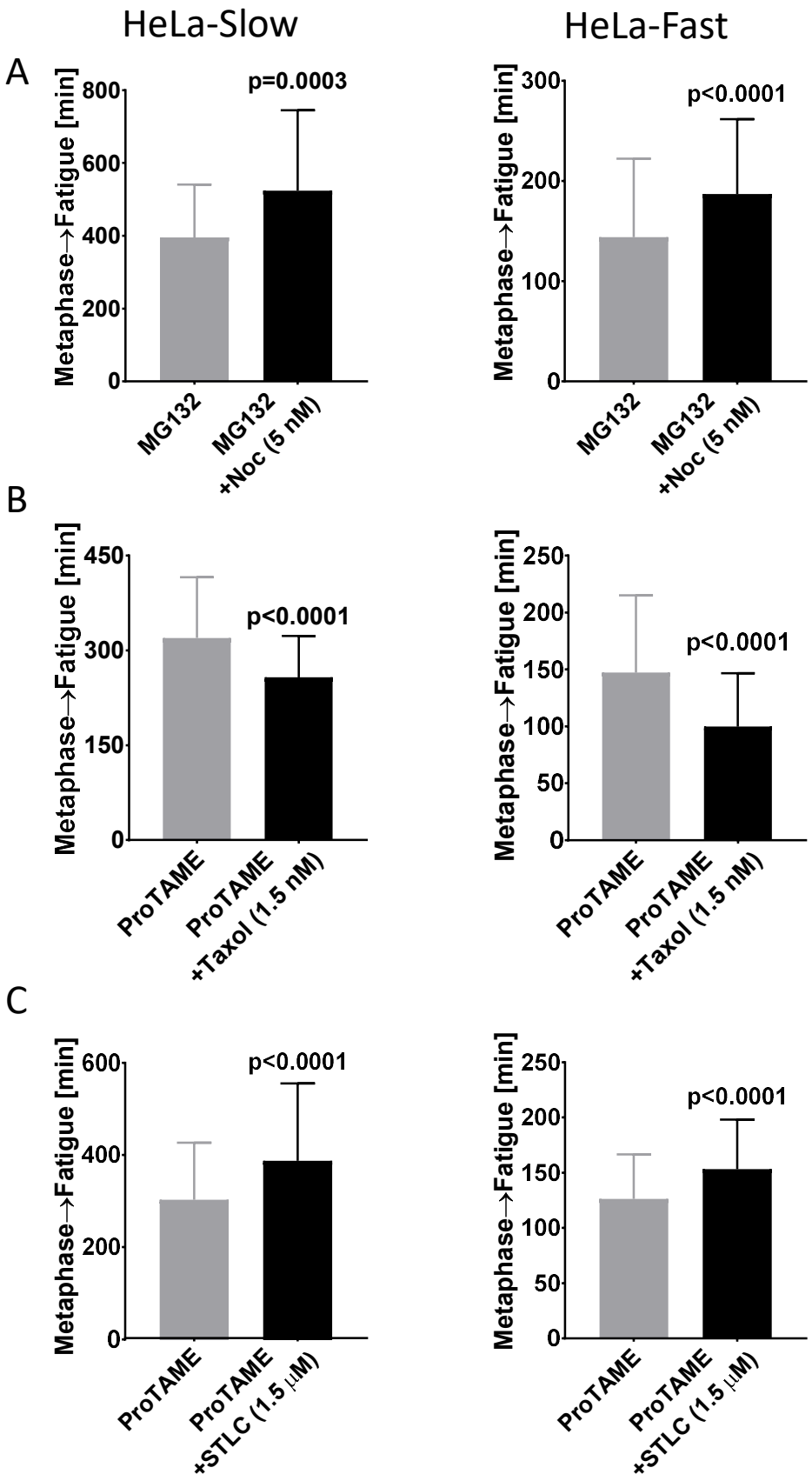
HeLa-Slow
HeLa-Fast
A
Metaphase→Fatigue [min]
p=0.0003
p<0.0001
MG132
MG132 +Noc (5 nM)
B
p<0.0001
p<0.0001
ProTAME
ProTAME +Taxol (1.5 nM)
C
p<0.0001
p<0.0001
ProTAME +STLC (1.5 μM)

Figure_5

A

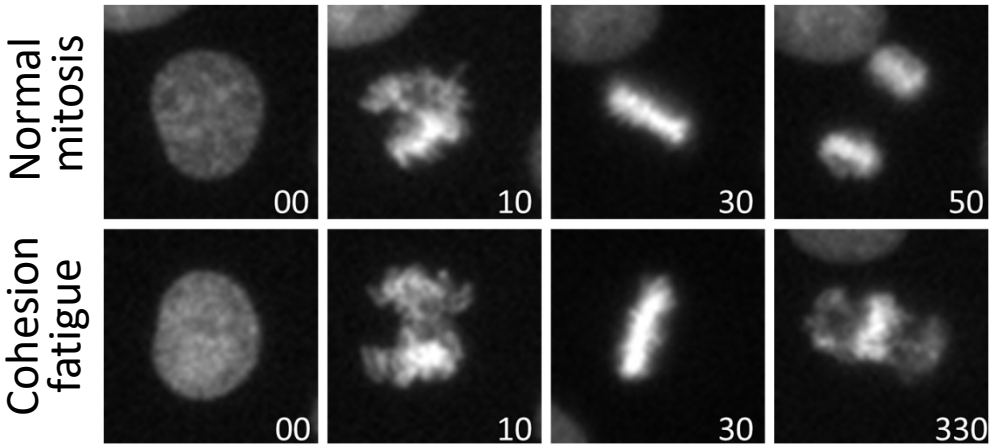
Normal mitosis
Cohesion fatigue
00
10
30
50
00
10
30
330

B

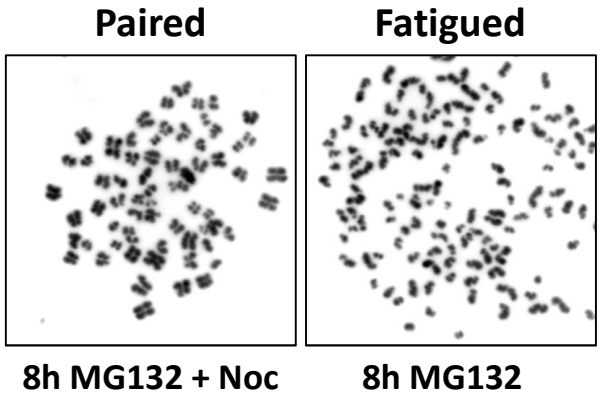
Paired
Fatigued
8h MG132 + Noc
8h MG132

figure_6

A

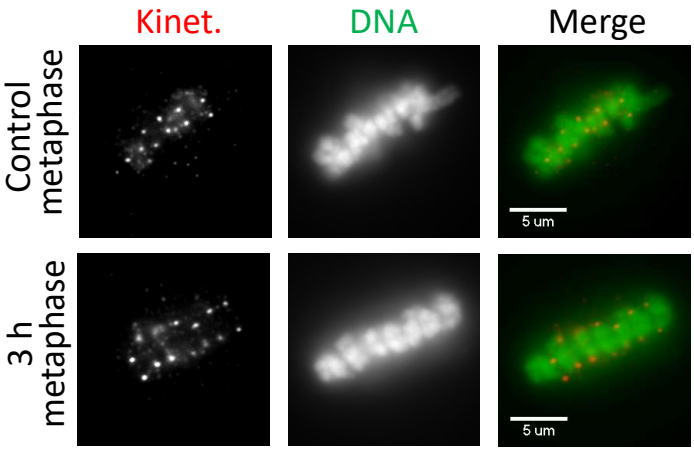
Kinet.
DNA
Merge
Control metaphase
3 h metaphase
5 um
5 um

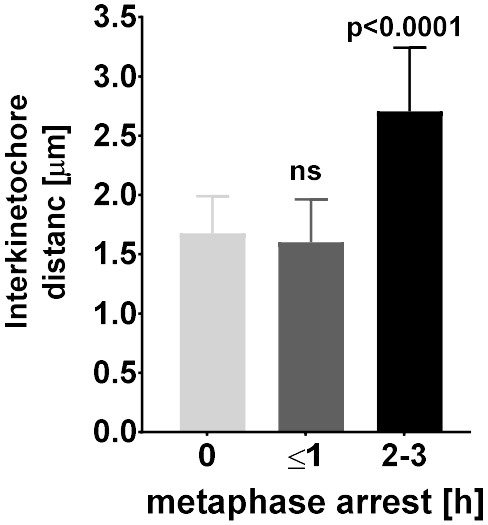
Interkinetochore distanc [µm]
3.5
3.0
2.5
2.0
1.5
1.0
0.5
0.0
p<0.0001
ns
0
≤1
2-3
metaphase arrest [h]

B

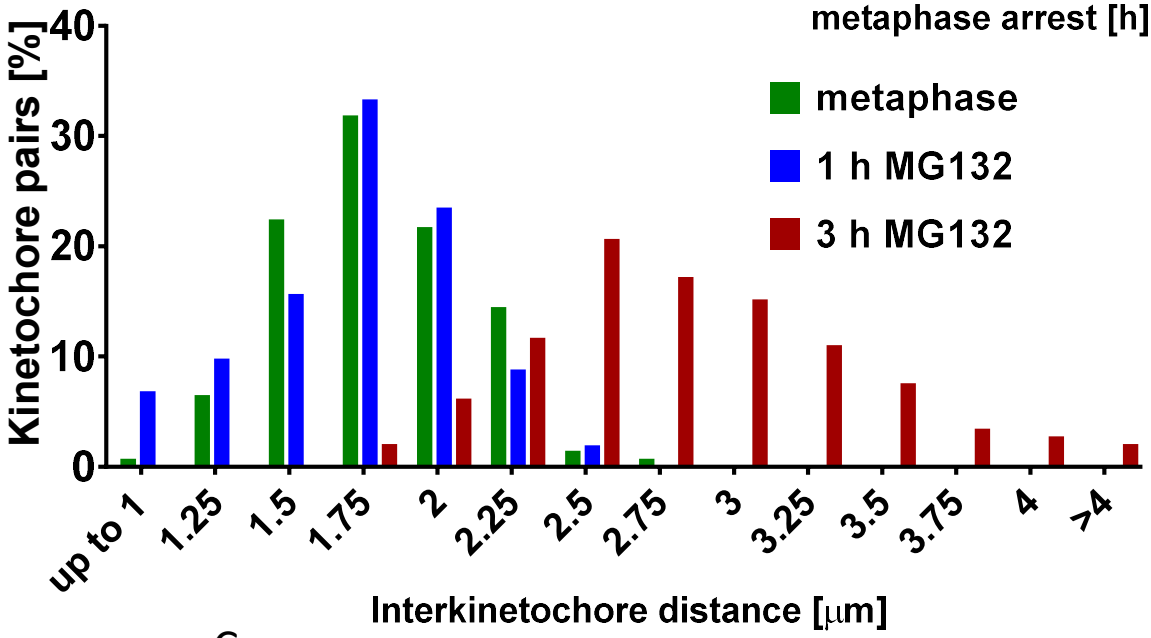
Kinetochore pairs [%]
40
30
20
10
0
metaphase
1 h MG132
3 h MG132
up to 1
1.25
1.5
1.75
2
2.25
2.5
2.75
3
3.25
3.5
3.75
4
>4
Interkinetochore distance [µm]

C

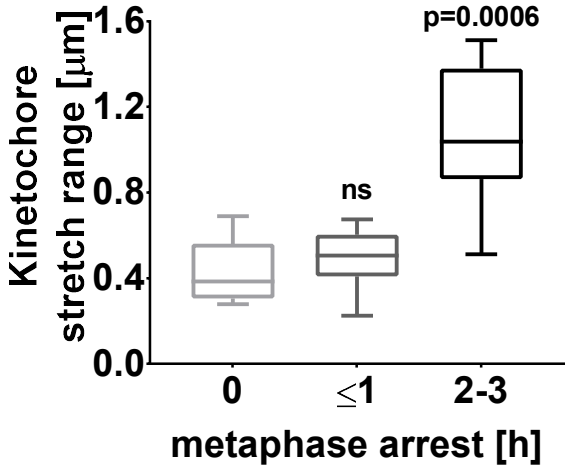
Kinetochore stretch range [µm]
1.6
1.2
0.8
0.4
0.0
p=0.0006
ns
0
≤1
2-3
metaphase arrest [h]

figure_7

A

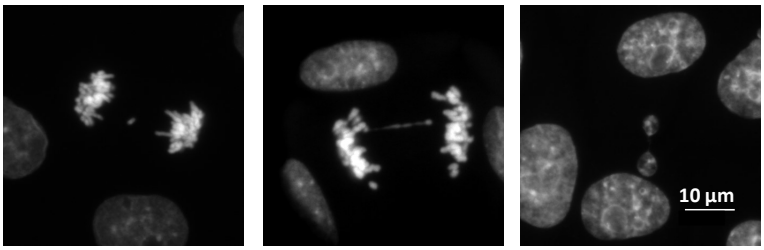

Lagging Anaphase bridge Micronuclei

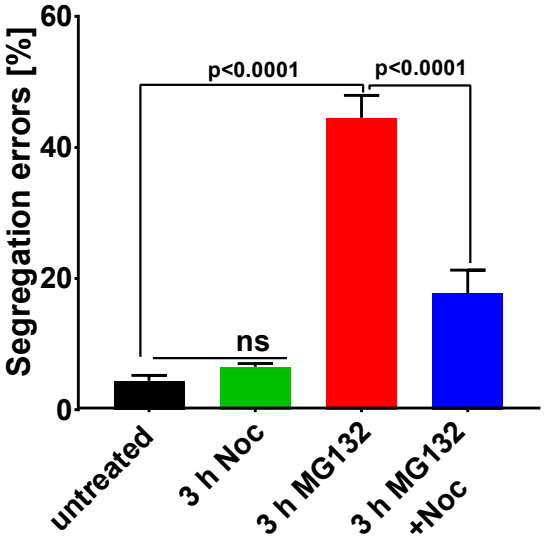

B

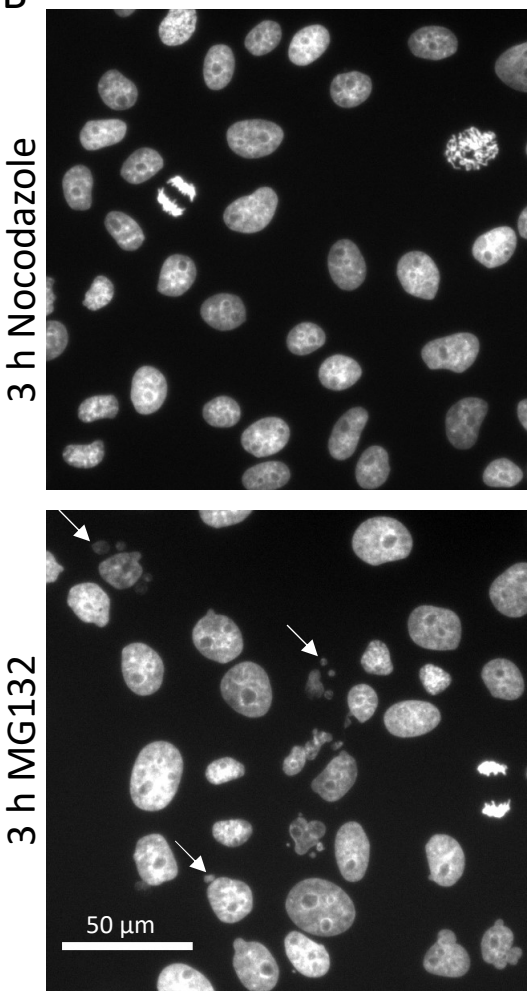

C

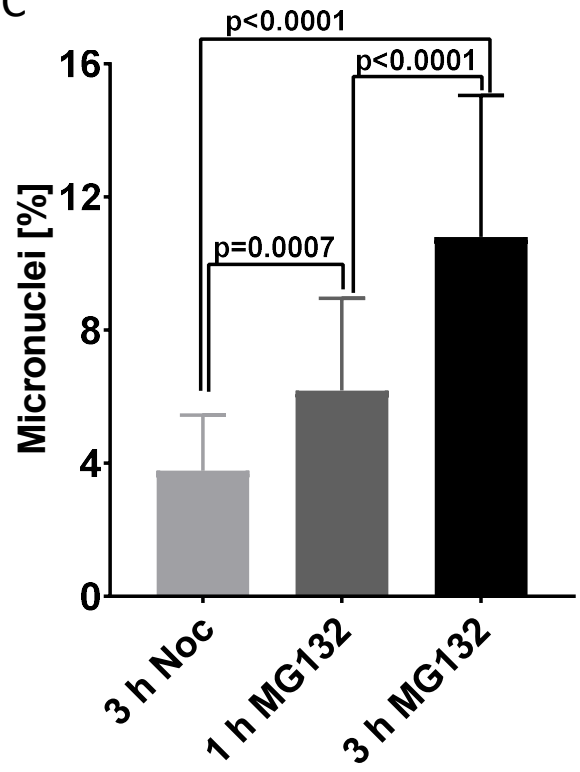

figure_8

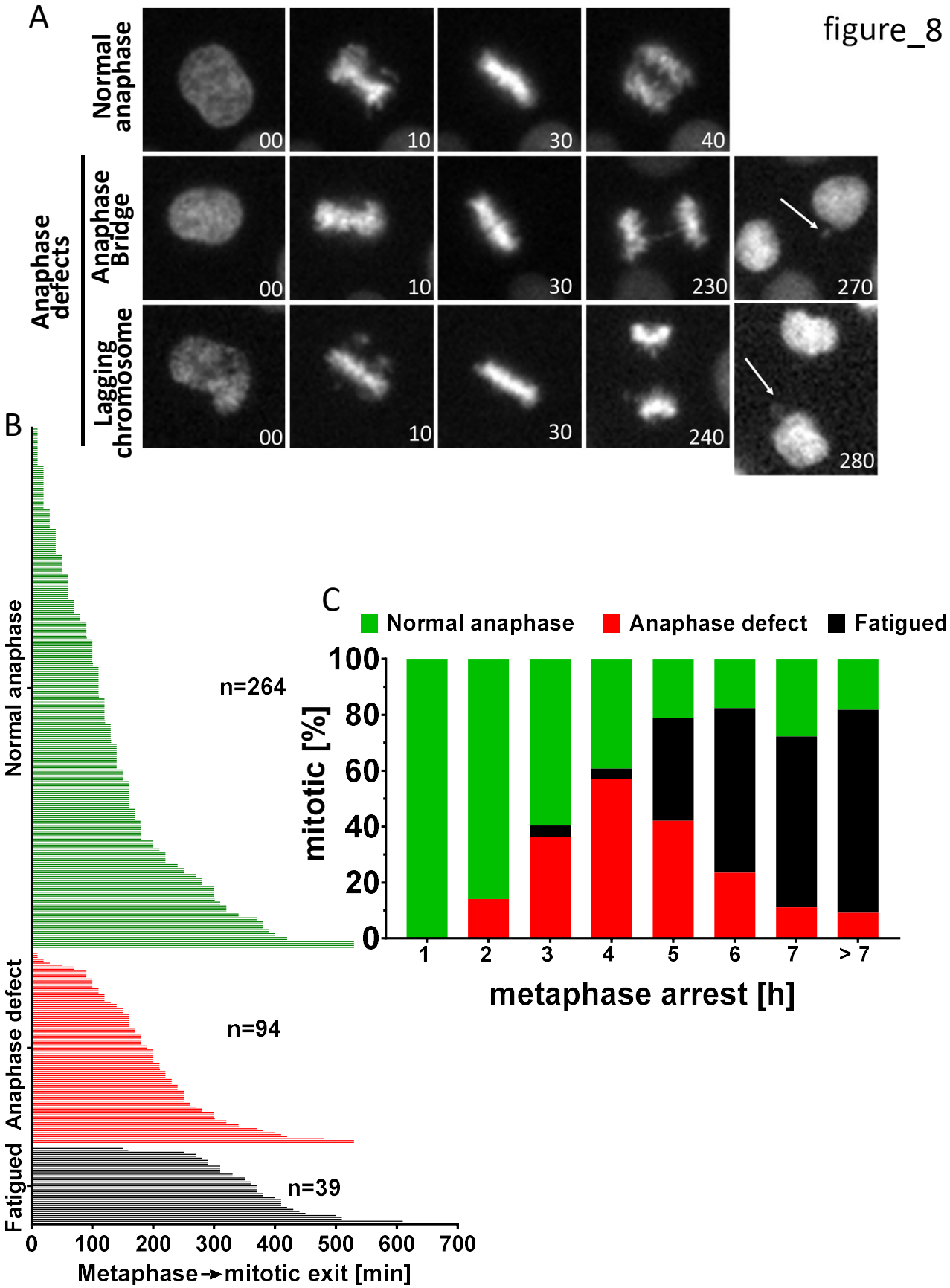
A
Normal anaphase
Anaphase defects
Anaphase Bridge
Lagging chromosome
00
10
30
40
230
240
270
280
B
Normal anaphase
Anaphase defect
Fatigued
n=264
n=94
n=39
0
100
200
300
400
500
600
700
Metaphase→mitotic exit [min]
C
Normal anaphase
Anaphase defect
Fatigued
mitotic [%]
100
80
60
40
20
0
1
2
3
4
5
6
7
> 7
metaphase arrest [h]